Plastic yield criterion and hardening of porous single crystals

Paux J., R. Brenner, D. Kondo

Plastic yield criterion and hardening of porous single crystals

J. Paux, R. Brenner*, D. Kondo

Sorbonne Universités, UPMC Univ Paris 06, CNRS, UMR 7190, Institut Jean le Rond d'Alembert, F-75005, Paris, France

Abstract

This article presents an assessment of the yield criterion for porous plastic single crystal, proposed by Paux et al. (2015), for face-centred cubic and hexagonal close-packed crystalline structures. Comparisons with reference FFT full-field computations on single voided cubic unit cells, presenting different crystal orientations, show an overall agreement for the different plastic anisotropies considered at low and high triaxiality. An extension of the criterion to hardenable crystals, which takes into account the spatial heterogeneity of the approximate plastic strain field, is further proposed and compared with FE results from the literature for body-centred cubic crystals.

Keywords: plasticity, single crystal, porosity, micromechanics

1. Introduction

The porosity evolution during the plastic deformation of metallic materials is known to play a dominating role in the fracture process. Voids are often initially present in the material due to the manufacturing process (infinitesimal porosity) or they can be created during the deformation due to the decohesion between precipitates and matrix phase. In any case, the description of void growth process requires to develop constitutive laws for the plastic response of porous crystalline materials with a special attention to the plastic anisotropy.

Although the importance of the crystalline anisotropy to describe the local stress field in the vicinity of intragranular voids has been clearly evidenced (Crépin et al., 1996; Gan et al., 2006; Schacht et al., 2003; Yerra et al., 2010; Srivastava and Needleman, 2013), relatively few works on the constitutive response of 3D plastic single crystals containing voids have been undertaken until recently. Based on the variational homogenization method of de Botton and Ponte Castañeda (1995) and guided by limit-analysis results, Han et al. (2013) have first proposed a yield function for 3D porous FCC single crystals containing spherical voids. Afterwards, we have proposed a model based on limit analysis which makes use of a regularized form of the Schmid law. It shares similarities with Han's model despite being derived with a different approach (Paux et al., 2015). Besides, by using on a "modified" variational method proposed by Danas and Aravas (2012), Mbiakop et al. (2015a) have developed a model for viscoplastic single crystals with ellipsoidal voids. Interestingly, the authors have also shown that these three models deliver very close estimates for rate-independent porous plasticity in the case of low plastic anisotropy (namely, face-centered cubic crystals) and spherical voids. Concerning the microstructural

*Corresponding author.
Email address: renald.brenner@upmc.fr (R. Brenner)

evolutions (void growth and strain hardening), it is worth mentioning the elastoviscoplastic model at finite strains proposed by Ling et al. (2016) based on the yield criterion of Han et al. (2013).

Following the study of Paux et al. (2015), the objective of the present article is threefold: firstly, the criterion is somewhat generalized to consider crystals with arbitrary symmetry and plastic anisotropy; secondly, the proposed criterion is assessed by comparison with several full-field computations performed on periodic microstructures by using a FFT-based numerical scheme (i.e. unit-cell computations) and, lastly, the extension of the proposed criterion to hardenable crystals, based on an approach of Leblond et al. (1995) for isotropic materials, is studied.

2. Yield criterion for the porous single crystal

2.1. Plastic yield criterion: Schmid law

We consider dislocation mediated plasticity of crystalline materials: plastic deformation occurs by dislocation glide on a set of K crystalline slip systems which depends on the specific crystalline structure. A slip system k is characterized by the unit normal to the slip plane $\mathbf{n}_k$ and the unit slip direction $\mathbf{m}_k$ ($\mathbf{m}_k.\mathbf{n}_k = 0$) which define the Schmid tensor $\boldsymbol{\mu}_k$

$$\boldsymbol{\mu}_k = \frac{1}{2}(\mathbf{n}_k \otimes \mathbf{m}_k + \mathbf{m}_k \otimes \mathbf{n}_k). \tag{2.1}$$

According to the Schmid law, a slip system k can be activated if the absolute value of the resolved shear stress $\tau_k = \boldsymbol{\sigma} : \boldsymbol{\mu}_k$ reaches a critical value τ_k^c. Because of this, the yield function of the single crystal is defined by a multi-criterion which reads

$$f(\boldsymbol{\sigma}) = \sup_{k=1,\dots,K} |\boldsymbol{\sigma} : \boldsymbol{\mu}_k| - \tau_k^c = \sup_{k=1,\dots,K} f_k(\boldsymbol{\sigma}) \tag{2.2}$$

As each criterion $f_k(\boldsymbol{\sigma}) = 0$ defines a plane in the space of deviatoric stress, the (pressure-insensitive) Schmid yield surface is a polyhedral surface whose shape depends on the geometry of the slip systems (Bishop and Hill, 1951; Kocks et al., 1983; Tomé and Kocks, 1985). The Schmid plastic domain is thus described as the convex hull of the polyhedron vertices.

For practical purpose, it can be advantageous to approximate this multi-criterion yield function by a single yield function as proposed, among others, by Arminjon (1991) and Gambin (1992),

$$f_{\text{reg}}^{(n)}(\boldsymbol{\sigma}) = \left(\sum_{k=1}^{K} \left(\frac{|\boldsymbol{\sigma} : \boldsymbol{\mu}_k|}{\tau_k^c} \right)^n \right)^{\frac{1}{n}} - 1 \tag{2.3}$$

where n is an exponent ≥ 2. As $n \to +\infty$, the regularized function $f_{reg}^{(n)}$ tends to the Schmid yield function f.

2.2. Approximate yield criterion using regularized Schmid law

An approximate yield criterion for porous crystals, previously derived in Paux et al. (2015), is briefly recalled and somewhat generalized with a view to extending it to hardenable materials (see Section 4).

2.2.1. Macroscopic yield surface of a hollow sphere

We aim to derive an approximation of the yield surface of rigid-perfectly plastic single crystals containing spherical voids by taking advantage of the regularized Schmid yield function (2.3). To this end, it is proposed to follow a kinematical limit-analysis approach for a single crystal sphere of radius b containing a confocal spherical void of radius a. The porosity p is defined as the ratio of the void volume ω over the sphere volume Ω

$$p = \frac{\omega}{\Omega} = \frac{a^3}{b^3}. \tag{2.4}$$

It is assumed that the sphere is subjected on its outer boundary $\partial\Omega$ to homogeneous strain rate conditions

$$\mathbf{v} = \mathbf{D}.\mathbf{x}, \quad \forall \mathbf{x} \in \partial\Omega, \tag{2.5}$$

with $\mathbf{v}$ the velocity field and $\mathbf{D}$ the macroscopic strain rate tensor. Besides, the single crystal presents a convex plastic strength domain $C^{(n)}$ defined by

$$C^{(n)} = \{\boldsymbol{\sigma} \text{ such that } f_{\text{reg}}^{(n)}(\boldsymbol{\sigma}) \leq 0\}. \tag{2.6}$$

According to the principle of maximum plastic work (Hill, 1950), the local plastic dissipation π reads

$$\pi(\mathbf{d}(\mathbf{x})) = \begin{cases} 0 & \text{if } \mathbf{x} \in \omega, \\ \sup\limits_{\boldsymbol{\sigma}^* \in C^{(n)}} \boldsymbol{\sigma}^* : \mathbf{d} & \text{if } \mathbf{x} \in \Omega - \omega. \end{cases} \tag{2.7}$$

with $\mathbf{d}$ the strain rate field (symmetric part of the gradient of the velocity field $\mathbf{v}$). In mathematics, π is called the support function of the convex domain $C^{(n)}$. For the porous material, the effective plastic dissipation function reads

$$\Pi(\mathbf{D}) = \inf_{\mathbf{v} \in \mathcal{K}(\mathbf{D})} \langle \pi \rangle_\Omega = (1-p) \inf_{\mathbf{v} \in \mathcal{K}(\mathbf{D})} \langle \pi \rangle_{\Omega - \omega}. \tag{2.8}$$

The notation $\langle . \rangle_V$ indicates a volume average over V and $\mathcal{K}$ is the set of kinematically admissible velocity fields

$$\mathcal{K}(\mathbf{D}) = \{\mathbf{v} \text{ such that } \mathbf{v}(\mathbf{x}) = \mathbf{D}.\mathbf{x}, \, \forall \mathbf{x} \in \partial\Omega, \text{ and } \operatorname{tr}(\mathbf{d}(\mathbf{x})) = 0, \forall \mathbf{x} \in \Omega - \omega\}. \tag{2.9}$$

The effective strength domain $\tilde{C}$ of the porous single crystal is defined as

$$\tilde{C} = \{\boldsymbol{\Sigma} \text{ such that } \boldsymbol{\Sigma} : \mathbf{D} \leq \Pi(\mathbf{D}), \, \forall \mathbf{D}\} \tag{2.10}$$

with $\boldsymbol{\Sigma}$ the macroscopic stress tensor. The corresponding macroscopic yield surface, defined as the boundary of the convex strength domain $\tilde{C}$, is thus given by

$$\boldsymbol{\Sigma} = \frac{\partial \Pi}{\partial \mathbf{D}}(\mathbf{D}). \tag{2.11}$$

Its derivation thus requires the determination of the support function $\pi(\mathbf{d})$ and to minimize its average over the sphere volume with respect to the velocity field. In general, the exact solution of the minimization problem is out of reach and a kinematically admissible velocity test field $\mathbf{v}_t$ is used. Since

$$\Pi(\mathbf{D}) = \inf_{\mathbf{v} \in \mathcal{K}(\mathbf{D})} \langle \pi \rangle_\Omega \leq \langle \pi(\mathbf{d}_t) \rangle_\Omega, \quad \mathbf{d}_t = \operatorname{sym}(\boldsymbol{\nabla} \mathbf{v}_t), \tag{2.12}$$

for any velocity test field $\mathbf{v}_t \in \mathcal{K}(\mathbf{D})$, relation (2.11) delivers an upper-bound for the yield surface. In the present study, we have chosen to use the test field initially proposed by Rice and Tracey (1969) which is the sum of an homogeneous deviatoric field and a field corresponding to the isotropic expansion of the hollow sphere. The velocity field, at point $\mathbf{x} = r\,\mathbf{e}_r$, then reads

$$\mathbf{v}_t(\mathbf{D}) = \mathbf{D}'.\mathbf{x} + \frac{b^3 D_m}{r^2}\boldsymbol{e}_r \tag{2.13}$$

with $\mathbf{D}'$ the deviatoric part of the macroscopic strain rate tensor and $D_m = (1/3)\mathrm{tr}\,(\mathbf{D})$ its hydrostatic part ($\mathbf{D} = \mathbf{D}' + D_m\mathbf{i}$). The corresponding strain rate field is

$$\mathbf{d}_t(\mathbf{D}) = \mathbf{D}' + \frac{b^3 D_m}{r^3}\mathbf{d}_m \tag{2.14}$$

with $\mathbf{d}_m = -2\mathbf{e}_r \otimes \mathbf{e}_r + \mathbf{e}_\varphi \otimes \mathbf{e}_\varphi + \mathbf{e}_\theta \otimes \mathbf{e}_\theta$ in spherical coordinates.

2.2.2. Approximate yield criterion

By using a quadratic regularized Schmid law (relation (2.3) with $n = 2$), the yield function can be put in the following form

$$f^{(2)}_{\mathrm{reg}}(\boldsymbol{\sigma}) = \sqrt{\boldsymbol{\sigma} : \mathbf{M} : \boldsymbol{\sigma}} - 1 \quad \text{with} \quad \mathbf{M} = \sum_{k=1}^{K} \frac{\boldsymbol{\mu}_k \otimes \boldsymbol{\mu}_k}{(\tau^c_k)^2}. \tag{2.15}$$

For crystals with at least orthotropic symmetry, the quadratic regularized criterion ($f^{(2)}_{\mathrm{reg}}(\boldsymbol{\sigma}) = 0$) corresponds to the Hill plastic criterion (Hill, 1948). Consequently, direct use can be made of previous results from the limit-analysis of a hollow sphere made of an anisotropic Hill matrix (Benzerga and Besson, 2001; Monchiet et al., 2008). The following quadratic criterion is thus obtained for single crystals containing spherical voids

$$\boldsymbol{\Sigma} : \mathbf{M} : \boldsymbol{\Sigma} + 2\,p\cosh\left(\kappa\Sigma_m\right) - 1 - p^2 = 0 \tag{2.16}$$

where κ is an anisotropy factor depending on $\mathbf{M}$[1]. As pointed out in Paux et al. (2015), in the case of face-centred cubic (FCC) crystals, this criterion leads to poor estimates for an arbitrary orientation of the crystal. A phenomenological improvement of this criterion has been proposed based on two specific loadings:

• *Case of a deviatoric macroscopic strain rate*

In the special case where $\mathbf{D} = \mathbf{D}'$, the computation of the overall plastic dissipation $\Pi(\mathbf{D})$ reads

$$\Pi(\mathbf{D}) = \frac{1}{\Omega}\int_{\Omega-\omega} \sup_{\boldsymbol{\sigma}^* \in C} \boldsymbol{\sigma}^* : \mathbf{D}'\ \mathrm{d}V \tag{2.17}$$

with C the space of plastically admissible stresses according to the Schmid law (i.e. $C = C^{(+\infty)}$). As mentioned above, C is a polyhedron and as such can be defined as the convex envelope of its vertices. The set of the vertices of C is noted $\mathcal{A}$. It depends on the geometry of the slip systems as well as

[1]The definitions of $\mathbf{M}$ and κ have been slightly modified here with respect to Paux et al. (2015) to account for slip systems with different CRSS. In the case of crystals with uniform CRSS ($\tau^c_k = \tau^c$), there is a factor τ^c for κ and $(\tau^c)^2$ for $\mathbf{M}$ between the two definitions.

their CRSS. Owing to the homogeneity of the strain rate field ($\mathbf{D}'$ is constant), relation (2.17) may be written as

$$\Pi(\mathbf{D}) = \frac{\Omega - \omega}{\Omega} \max_{\boldsymbol{\sigma}^* \in \mathcal{A}} \boldsymbol{\sigma}^* : \mathbf{D}' = (1-p) \max_{\boldsymbol{\sigma}^* \in \mathcal{A}} \boldsymbol{\sigma}^* : \mathbf{D}' \tag{2.18}$$

and the macroscopic yield stress is given by

$$\boldsymbol{\Sigma} = \frac{\partial \Pi}{\partial \mathbf{D}}(\mathbf{D}) = (1-p)\, \mathrm{argmax}_{\boldsymbol{\sigma}^* \in \mathcal{A}} (\boldsymbol{\sigma}^* : \mathbf{D}') \tag{2.19}$$

Since $\mathbf{D}'$ is any deviatoric strain rate tensor, it follows that the macroscopic yield surface is the convex hull of $(1-p)\mathcal{A} = \{(1-p)\boldsymbol{\sigma},\ \boldsymbol{\sigma} \in \mathcal{A}\}$. Thereby, the plastic yield function of a porous crystal, for deviatoric macroscopic stresses ($\Sigma_m = 0$), takes the form

$$\mathcal{F}(\boldsymbol{\Sigma}) = \sup_{k=1,\ldots,K} \frac{|\boldsymbol{\Sigma} : \boldsymbol{\mu}_k|}{\tau_k^c} - (1-p). \tag{2.20}$$

Besides, it is noted that a regularized local plastic strength domain $C^{(n)}$ (2.6) leads to the following macroscopic yield function

$$\mathcal{F}_{\mathrm{reg}}^{(n)}(\boldsymbol{\Sigma}) = \left(\sum_{k=1}^{K} \left(\frac{|\boldsymbol{\Sigma} : \boldsymbol{\mu}_k|}{\tau_k^c} \right)^n \right)^{\frac{1}{n}} - (1-p) \tag{2.21}$$

which conspicuously coincides with $\mathcal{F}(\boldsymbol{\Sigma})$ as $n \to \infty$.

• *Case of a hydrostatic macroscopic strain rate*

In the special case where $\mathbf{D} = D_m \mathbf{i}$, the overall plastic dissipation reads

$$\begin{aligned} \Pi(\mathbf{D}) &= \frac{b^3 |D_m|}{\Omega} \int_{\Omega - \omega} \frac{1}{r^3} \max_{\boldsymbol{\sigma}^* \in \mathcal{A}} \boldsymbol{\sigma}^* : \mathbf{d}_m \, \mathrm{d}V \\ &= \frac{3|D_m|}{4\pi} \int_a^b \frac{\mathrm{d}r}{r} \underbrace{\int_{\varphi=0}^{\pi} \int_{\theta=0}^{2\pi} \max_{\boldsymbol{\sigma}^* \in \mathcal{A}} \boldsymbol{\sigma}^* : \mathbf{d}_m \sin\varphi \, \mathrm{d}\varphi \, \mathrm{d}\theta}_{I_\Pi} = -\frac{I_\Pi |D_m| \ln p}{4\pi} \end{aligned} \tag{2.22}$$

The double integral I_Π is evaluated numerically by using Gauss-Legendre quadrature. For each angular position (φ, θ), it involves the computation of the maximum value of $\boldsymbol{\sigma}^* : \mathbf{d}_m$ on the finite set $\mathcal{A}$ corresponding to the stress vertices of the polyhedral yield surface. The limit-analysis numerical estimate of the macroscopic mean yield stress is thus

$$\Sigma_m = \frac{1}{3} \frac{\partial \Pi}{\partial D_m}(\mathbf{D}) = -\frac{I_\Pi \ln p}{12\pi} \mathrm{sgn}(D_m) \tag{2.23}$$

On the other hand, the form of the criterion (2.16) gives $\Sigma_m = -\ln p / \kappa$ so that the κ parameter reads $\kappa = 12\pi / I_\Pi$.

Based on the results for purely deviatoric and hydrostatic loadings, the following criterion is proposed, as a phenomenological extension of the quadratic criterion (2.16),

$$\mathcal{F}(\boldsymbol{\Sigma}) = \left(\sup_{k=1,\ldots,K} \frac{|\boldsymbol{\Sigma} : \boldsymbol{\mu}_k|}{\tau_k^c} \right)^2 + 2p \cosh(\kappa \Sigma_m) - 1 - p^2. \tag{2.24}$$

Its regularized form reads

$$\mathcal{F}_{\text{reg}}^{(n)}(\boldsymbol{\Sigma}) = \left(\sum_k \left(\frac{|\boldsymbol{\Sigma} : \boldsymbol{\mu}_k|}{\tau_k^c} \right)^n \right)^{\frac{2}{n}} + 2p \cosh(\kappa\, \Sigma_m) - 1 - p^2. \tag{2.25}$$

In view of the assessment of this criterion, obtained for a hollow sphere, for materials with a periodic microstructure (unit-cell computations), a fitting parameter $q \geq 1$ is customarily introduced (Tvergaard, 1982). It introduces a so-called enhanced porosity qp. The regularized criterion is finally expressed as

$$\mathcal{F}_{\text{reg}}^{(n)}(\boldsymbol{\Sigma}) = \left(\sum_k \left(\frac{|\boldsymbol{\Sigma} : \boldsymbol{\mu}_k|}{\tau_k^c} \right)^n \right)^{\frac{2}{n}} + 2qp \cosh(\kappa\, \Sigma_m) - 1 - (qp)^2. \tag{2.26}$$

It is pointed out that the evaluation of κ results from a numerical limit-analysis calculation on a single crystal hollow sphere. It thus requires the knowledge of the set of vertices $\mathcal{A}$ of the polyhedral yield surface which depends on the crystalline structure and on the ratios of the CRSS on the different slip systems. An increase of the single crystal plastic anisotropy, which especially depends on the ratios of the critical shear stresses, leads to an increase of the I_Π integral (i.e. decrease of the κ parameter; see the reported values for specific crystalline structures in Section 3.2.1). As a consequence, the higher the plastic anisotropy, the higher the yield strength under hydrostatic loading. Interestingly, it has been recently reported that "highly anisotropic" porous crystal are incompressible (Mbiakop et al., 2015a,b). More specifically, it can be proven that low-symmetry crystals *lacking five independent slip systems* exhibit this property (Appendix A). This situation corresponds to an infinite plastic anisotropy (i.e. opened yield surface in the deviatoric space). Our criterion is consistent, by construction, with this result since in this case $\kappa = 0$ (i.e infinite yield strength under hydrostatic loading). It is worth noting that, in the context of polycrystalline materials with *intergranular* porosity, Nervi and Idiart (2015) have recently shown that the self-consistent scheme predicts that voided polycrystals made of constitutive crystals with only three independent slip systems are still compressible.

3. Numerical assessment of the criterion

To evaluate the accuracy of the proposed criterion (2.26), full-field numerical computations have been performed on single crystals containing a cubic array of spherical voids. This is the purpose of the present section. It is emphasized that the yield surface of the porous single crystal is determined numerically by considering a fixed microstructure (no porosity evolution). The yield stress is defined as the stationary value of the macroscopic stress in the plastic regime. The microstructure being periodic, we can classically consider a local elastoplastic problem on a unit-cell with periodic boundary conditions. To solve this problem, use has been made of the FFT method (Moulinec and Suquet, 1998; Eyre and Milton, 1999; Suquet et al., 2012; Monchiet and Bonnet, 2012; Moulinec and Silva, 2014) which is an attractive alternative to the finite-element method. The numerical code has been built upon the one developed by Brenner et al. (2009) and Belkhabbaz et al. (2011, 2015) for rate-independent crystalline elastoplasticity.

3.1. Full-field unit-cell computations

3.1.1. Local problem

We consider a single crystal cubic volume V, with outer boundary ∂V, containing a spherical void. The infinite medium is described by the periodical arrangement of this unit-cell. The local problem to

solve on the unit-cell with prescribed macroscopic strain $\overline{\boldsymbol{\varepsilon}}(t) = \langle \boldsymbol{\varepsilon}(t) \rangle_V$, $t \in [0; t_f]$, reads: find $\mathbf{u}(\mathbf{x}, t)$ and $\boldsymbol{\sigma}(\mathbf{x}, t)$ such that

$$\left\{ \begin{array}{rcll} \boldsymbol{\varepsilon}(\mathbf{x},t) & = & \dfrac{1}{2}(\boldsymbol{\nabla}\mathbf{u}(\mathbf{x},t) + \boldsymbol{\nabla}\mathbf{u}^{\mathrm{T}}(\mathbf{x},t)), & \forall (\mathbf{x},t) \in V \times [0;t_f] \\ \dot{\boldsymbol{\sigma}}(\mathbf{x},t) & = & \mathbf{C}(\mathbf{x}) : (\dot{\boldsymbol{\varepsilon}}(\mathbf{x},t) - \dot{\boldsymbol{\varepsilon}}^p(\mathbf{x},t)), \quad \mathrm{div}\, \boldsymbol{\sigma}(\mathbf{x},t) = \mathbf{0}, & \forall (\mathbf{x},t) \in V \times [0;t_f] \\ \mathbf{u}(\mathbf{x},t) & = & \overline{\boldsymbol{\varepsilon}}(t).\mathbf{x} + \mathbf{u}'(\mathbf{x},t),\ \mathbf{u}' \text{ periodic on } \partial V, & \forall t \in [0;t_f]. \end{array} \right. \tag{3.1}$$

Besides, according to the principle of maximum plastic work, the plastic strain rate corresponding to the Schmid criterion is given by

$$\dot{\boldsymbol{\varepsilon}^p} = \sum_{k=1}^{K} \dot{\gamma}_k \frac{\partial f_k}{\partial \boldsymbol{\sigma}} = \sum_{k=1}^{K} \dot{\gamma}_k\, \boldsymbol{\mu}_k\, \mathrm{sgn}(\tau_k) \quad \text{with} \quad \dot{\gamma}_k \geq 0,\ \dot{\gamma}_k f_k(\boldsymbol{\sigma}) = 0,\ \forall k \in [1;K]. \tag{3.2}$$

The heterogeneous elastoplastic problem is solved incrementally by discretizing the time interval $[0; t_f]$. Suppose that the problem has been solved at time t_{i-1}. The stress and strain fields at time t_i, for a prescribed overall strain increment $\Delta\overline{\boldsymbol{\varepsilon}}$, are determined by using a FFT numerical scheme for a composite material with a nonlinear local constitutive law of the form

$$\boldsymbol{\sigma}_i(\mathbf{x}) = F(\boldsymbol{\varepsilon}_i(\mathbf{x}), \mathbf{x}) \tag{3.3}$$

which is obtained by the time-integration of the differential constitutive relation. The principle of the FFT-based numerical algorithm is not reminded here since a wide literature exists on this topic for composites and polycrystalline materials (see, among others, Moulinec and Suquet, 1998; Lebensohn, 2001; Brenner et al., 2009; Suquet et al., 2012; Belkhabbaz et al., 2015, and references therein). Moreover, for voided materials, the reader is more specifically referred to the works of Michel et al. (2001); Willot and Pellegrini (2008); Brisard and Dormieux (2010); Vincent et al. (2014).

3.1.2. Stress update algorithm

The time-integration of the local (rate-independent) constitutive relation is as follows. The unit-cell being discretized into $N \times N \times N$ voxels, it is assumed that the voxel-wise stress and strain tensors at time t_{i-1} ($\boldsymbol{\sigma}_{i-1}$, $\boldsymbol{\varepsilon}_{i-1}$) are known, as well as a guess for the field of total strain increment $\Delta\boldsymbol{\varepsilon} = \boldsymbol{\varepsilon}_i - \boldsymbol{\varepsilon}_{i-1}$. The problem is then to compute the local stress field $\boldsymbol{\sigma}_i(\boldsymbol{\varepsilon}_i)$ at each voxel of the unit-cell.

Case of perfect plasticity :
The critical resolved shear stresses τ_k^c ($\forall k = 1, \ldots, K$) are constant. Let $\boldsymbol{\sigma}^e$ be the stress elastic guess, that is $\boldsymbol{\sigma}^e = \boldsymbol{\sigma}_{i-1} + \mathbf{C} : \Delta\boldsymbol{\varepsilon}$. Two cases must be considered in practice:

- $\max\limits_{k=1,\ldots,K} f_k(\boldsymbol{\sigma}^e) < 0$

  The behaviour is elastic and the solution is $\boldsymbol{\sigma} = \boldsymbol{\sigma}^e$ and $\Delta\boldsymbol{\varepsilon}^p = 0$.

- $\max\limits_{k=1,\ldots,K} f_k(\boldsymbol{\sigma}^e) > 0$

  The behaviour is elastoplastic. The stress $\boldsymbol{\sigma}$ and the plastic strain increment $\Delta\boldsymbol{\varepsilon}^p$ are solutions of

$$\left\{ \begin{array}{rcl} f(\boldsymbol{\sigma}) & = & \max\limits_{k=1,\ldots,K} f_k(\boldsymbol{\sigma}) \ = \max\limits_{k=1,\ldots,K} |\boldsymbol{\mu}_k : \boldsymbol{\sigma}| - \tau_k^c \ = \ 0, \\ \boldsymbol{\sigma} & = & \boldsymbol{\sigma}^e - \mathbf{C} : \Delta\boldsymbol{\varepsilon}^p, \\ \Delta\boldsymbol{\varepsilon}^p & = & \displaystyle\sum_{k=1}^{K} \Delta\gamma_k \frac{\partial f_k}{\partial \boldsymbol{\sigma}}(\boldsymbol{\sigma}), \quad \Delta\gamma_k \geq 0, \quad \Delta\gamma_k f_k = 0. \end{array} \right. \tag{3.4}$$

By introducing the function $g(\boldsymbol{\sigma})$ such that

$$\Delta\boldsymbol{\varepsilon}^p = \frac{\partial g}{\partial \boldsymbol{\sigma}}(\boldsymbol{\sigma}) = \mathbf{C}^{-1} : (\boldsymbol{\sigma}^{\boldsymbol{e}} - \boldsymbol{\sigma}), \tag{3.5}$$

$\boldsymbol{\sigma}$ is equivalently solution of the optimization problem

$$\begin{cases} \min\limits_{\boldsymbol{\sigma}} g(\boldsymbol{\sigma}) \quad \text{with} \quad \max\limits_{k=1,\dots,K} f_k(\boldsymbol{\sigma}) = 0, \\ \\ g(\boldsymbol{\sigma}) = \dfrac{1}{2}(\boldsymbol{\sigma}^{\boldsymbol{e}} - \boldsymbol{\sigma}) : \mathbf{C}^{-1} : (\boldsymbol{\sigma}^{\boldsymbol{e}} - \boldsymbol{\sigma}). \end{cases} \tag{3.6}$$

The corresponding Lagrangian function reads

$$\mathcal{L}(\boldsymbol{\sigma}, \Delta\gamma_k) = g(\boldsymbol{\sigma}) - \sum_{k=1}^{K} \Delta\gamma_k f_k(\boldsymbol{\sigma}). \tag{3.7}$$

Optimality with respect to the plastic slip increments $\Delta\gamma_k$ ensures that the stress is plastically admissible whereas the optimality with respect to the stress implies (generalized normality rule)

$$\Delta\boldsymbol{\varepsilon}^p = \frac{\partial g}{\partial \boldsymbol{\sigma}}(\boldsymbol{\sigma}) = \sum_{k=1}^{K} \Delta\gamma_k \frac{\partial f_k}{\partial \boldsymbol{\sigma}}(\boldsymbol{\sigma}). \tag{3.8}$$

Since the plastic yield function defines a polyhedron in the (deviatoric) stress space, the optimization problem (3.6) can be solved numerically by using the gradient projection method (Rosen, 1960). It consists in successive projections of the gradient of g onto hyperplanes defining the Schmid criterion (linear constraints on $\boldsymbol{\sigma}$ for the optimization problem). At each step, the algorithm provides a new direction to minimize g while remaining on the yield surface.

The plastic strain increment is uniquely defined by

$$\Delta\boldsymbol{\varepsilon}^p = \mathbf{C}^{-1} : (\boldsymbol{\sigma}^{\boldsymbol{e}} - \boldsymbol{\sigma}) \tag{3.9}$$

but the corresponding set of plastic slip increments $(\Delta\gamma_k)$, which is not needed to update the stress field in the case of perfect plasticity, is not unique in general.

3.2. Evaluation of the approximate yield criterion

3.2.1. Crystalline structures

To investigate different plastic anisotropies, we have considered face-centred cubic (FCC) and hexagonal close-packed (HCP) crystalline structures. Many common metallic alloys present one of these two dense crystalline structures: for instance, Cu, Al, stainless steels are FCC while Ti, Mg, Zn and Zr alloys are HCP. The other widely present structure is body-centred cubic (BCC). However, it will not be considered since it presents slip systems and a (low) plastic anisotropy similar to the ones of the FCC structure. The plastic anisotropy of the single crystal depends on the set of slip systems and on the ratios between the different critical shear stresses. FCC crystals present 12 octahedral slip systems $\{111\} < 110 >$. Since there is a single family of crystallographically equivalent slip systems, the accuracy of the criterion is independent of the value of the CRSS. In contradistinction, HCP crystals present different slip system families and a more pronounced plastic anisotropy. The latter critically depends on the CRSS ratios between the different families which vary from one metal to another. To a lower

extent, the geometry of the slip system varies with the c/a ratio of the hexagonal lattice parameters which, in general, slightly differ from the dense-packing ideal value ($\sqrt{8/3}$). For the HCP crystals, three main slip systems families exist: prismatic slip $\{10\bar{1}0\} < 1\bar{2}10 >$, basal slip $\{0001\} < 1\bar{2}10 >$ and pyramidal slip $\{10\bar{1}1\} < \bar{2}113 >$ (Groves and Kelly, 1963; Partridge, 1967; Yoo, 1981; Tomé and Kocks, 1985). HCP metals present either the prismatic or the basal slip as easy deformation mode. These two cases are considered in the present study with on one hand Ti crystals and on the other hand Mg crystals. The following CRSS ratios, respectively taken from Fundenberger et al. (1997) and Agnew et al. (2006) have been used

$$\begin{cases} \mathrm{HCP_{Ti}} & : \quad \dfrac{\tau^c_{Pyr.}}{\tau^c_{Pr.}} = 8, \qquad \dfrac{\tau^c_{Bas.}}{\tau^c_{Pr.}} = 5 \\ \mathrm{HCP_{Mg}} & : \quad \dfrac{\tau^c_{Pyr.}}{\tau^c_{Bas.}} = 6, \qquad \dfrac{\tau^c_{Pr.}}{\tau^c_{Bas.}} = 5.5 \end{cases} \tag{3.10}$$

For each crystalline structure, the κ anisotropy parameter entering the criterion (2.25) has been evaluated. It must be noted that the value obtained for the FCC crystal ($\kappa = 0.49$), slightly differs from the one previously reported in Paux et al. (2015) ($\kappa = 0.506$) due to a numerical error in our previous computation of I_Π. As the anisotropy of the yield surface increases (see the study of Tomé and Kocks (1985) for the particular case of hexagonal crystals), the numerical estimate of I_Π (and thus the mean yield stress Σ_m) increases since "hard" slip systems must be activated at certain points of the sphere to accomodate the overall prescribed rate of volume change $\dot{\Omega}/\Omega = 3D_m$. As a result, the anisotropy parameter decreases when the plastic anisotropy increases (Table 1). Note that in the case of a von Mises material (i.e. Gurson criterion), the $\bar{\kappa}$ parameter is equal to $3/2$.

	FCC	$\mathrm{HCP_{Mg}}$	$\mathrm{HCP_{Ti}}$
$\bar{\kappa}$	0.49	0.14	0.13

Table 1: Values of the normalized anisotropy parameter $\bar{\kappa} = \kappa \min \tau^c_k$ for different single crystal materials.

3.2.2. Unit-cell computations

To evaluate the proposed criterion, the elastoplastic response (without hardening) of single crystals containing a cubic periodic distribution of spherical voids has been computed for different crystal orientations. The simulations have been performed by using the FFT numerical scheme on a unit-cell constituted of a single crystal matrix with a spherical void. The test is strain driven but the macroscopic stress direction is imposed (see Moulinec and Suquet, 1998, Appendix B). In the unit-cell reference frame, the considered macroscopic stress tensor reads

$$\boldsymbol{\Sigma} = \Sigma_I \begin{pmatrix} \eta_1 & 0 & 0 \\ 0 & \eta_2 & 0 \\ 0 & 0 & 1 \end{pmatrix}. \tag{3.11}$$

The stress triaxiality T thus reads

$$T = \frac{\Sigma_m}{\Sigma_{eq}} = \frac{\sqrt{2}}{3} \frac{1 + \eta_1 + \eta_2}{\sqrt{(1-\eta_1)^2 + (1-\eta_2)^2 + (\eta_1 - \eta_2)^2}} \tag{3.12}$$

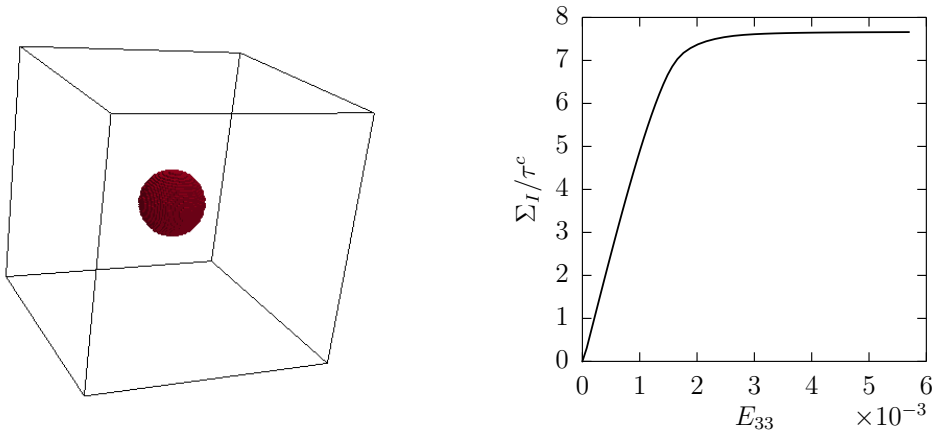

(a) (b)

Figure 1: Unit-cell with 1% porosity (a) and FFT macroscopic response for a FCC crystal subjected to axisymmetric stress state with $\eta = 0.8$ ($T = 13/3$) along [001] (b).

and the Lode parameter L, a measure of the third stress invariant, (see, for instance, Zhang et al., 2001)

$$L = \frac{2\eta_1 - 1 - \eta_2}{1 - \eta_2} \tag{3.13}$$

ranges from -1 to 1. $L = -1$ corresponds to triaxial tension, $L = 0$ to shear and $L = 1$ to triaxial compression. For each loading case, the yield stress is defined as the stationary value of the macroscopic stress Σ_I (Figure 1). Preliminary calculations have been performed for FCC crystals with few specific orientations by considering a discretization of the unit cell of $128 \times 128 \times 128$ voxels. The FFT results compared well with published finite-element results (Han et al., 2013) for a porosity ranging from 1 to 10%. Then, coarser grids have been used and no significant differences have been observed down to a discretization of $40 \times 40 \times 40$. The results presented hereafter have been obtained with this latter grid.

Two types of tests have been considered:

- Axisymmetric loading tests ($\eta_1 = \eta_2 = \eta$) for several crystal orientations so that the loading axis varies in the irreducible orientation space (i.e. standard spherical triangle) of each crystalline structure. In this case, the Lode parameter is fixed ($L = -1$) and the stress triaxiality is $T = (1 + 2\eta)/3(1 - \eta)$ with $\eta \in [-0.5; 1]$ ($\eta = -0.5$ corresponds to a purely deviatoric loading and $\eta = 1$ to a purely hydrostatic one). Four values of the porosity have been chosen (1, 2, 5 and 10%).

- Non-axisymmetric loading tests ($\eta_1 \neq \eta_2$) for different crystal orientations at fixed triaxiality T and variable Lode parameter L. Four crystal orientations have been chosen, from high to low symmetry: [100][010][001], [100][01$\bar{1}$][011], [110][$\bar{1}1\bar{2}$][$\bar{1}11$] and [5$\bar{2}$1][12$\bar{1}$][012]. Three triaxialities are considered: $T = 0$, 1/3 and 13/3. The evolution of η_1 and η_2 as a function of the Lode parameter, for each triaxiality, is given in Figure 2. A porosity $p = 1\%$ has been considered.

3.2.3. Results for FCC crystals

For the axisymmetric tests, 92 FFT computations have been performed with different crystal orientations, for each porosity value, so that the loading axis spans the whole standard spherical triangle.

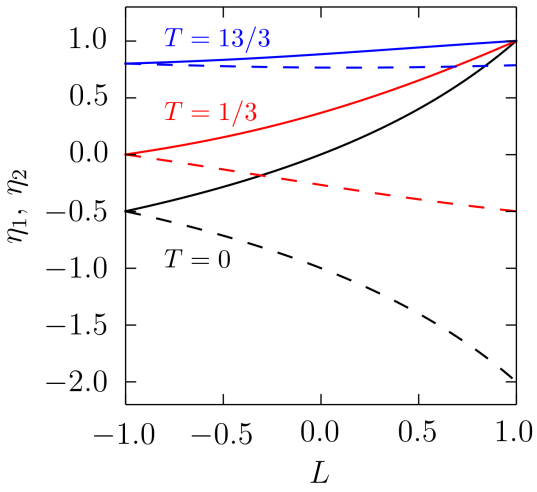

Figure 2: η_1 (solid line) and η_2 (dotted line) parameters (3.11) as a function of the Lode parameter for three triaxialities ($T = 0$, 1/3 and 13/3).

These reference numerical results have been used to fit the unique parameter of our criterion (q). The best overall agreement has been obtained with $q = 2$. It is noted that this parameter is rather insensitive to the porosity value. Comparisons are reported, for different triaxialities, on Figure 3. A correct description of the orientation dependence of the yield stress is obtained for $\eta \in [-0.5; 1[$ with a maximum relative error of 5%. Besides, the predicted hydrostatic yield stress ($\eta = 1$) is in close agreement with the FFT numerical results. Similar results, not shown here for brevity, have been obtained up to 10% porosity. It can be observed that the unit-cell computations exhibit a slight orientation dependence, for an hydrostatic loading, unlike the analytical criterion derived for a hollow sphere. This is due to the fact that the crystalline matrix is rotated with respect to the reference frame, for the different unit-cell calculations, while the cubic array of spherical voids is not. Consequently, the relative directions of anisotropy of the microstructure and the crystal change with the crystal orientation. This results in different periodic materials. The hydrostatic response is mainly affected by this microstructural change.

Following these assesments, we have considered non-axisymmetric stress loadings for four fixed crystal orientations, from high ([100][010][001]) to low ([5$\bar{2}$1][12$\bar{1}$][012]) symmetry, and a porosity of 1%. Moreover, the stress triaxiality is kept constant and the Lode parameter L varies. The evolution of the normalized yield stress with L is shown in Figures 4 to 6. An overall agreement is obtained for the different crystal orientations. It is pointed out that the abrupt changes of the yield stress evolution is related to the activation of different slip systems. However, at high stress triaxiality, the agreement worsens. This is likely related, at least partially, to the discrepancy between the actual plastic strain rate field (Figure 9a) and the trial strain rate field that we used (constant deviatoric term plus an isochoric isotropic growth).

3.2.4. Results for HCP crystals

For the two types of hexagonal crystals considered (Ti-like and Mg-like), 89 FFT computations have been carried out to vary the orientation of the loading axis in the standard spherical triangle.

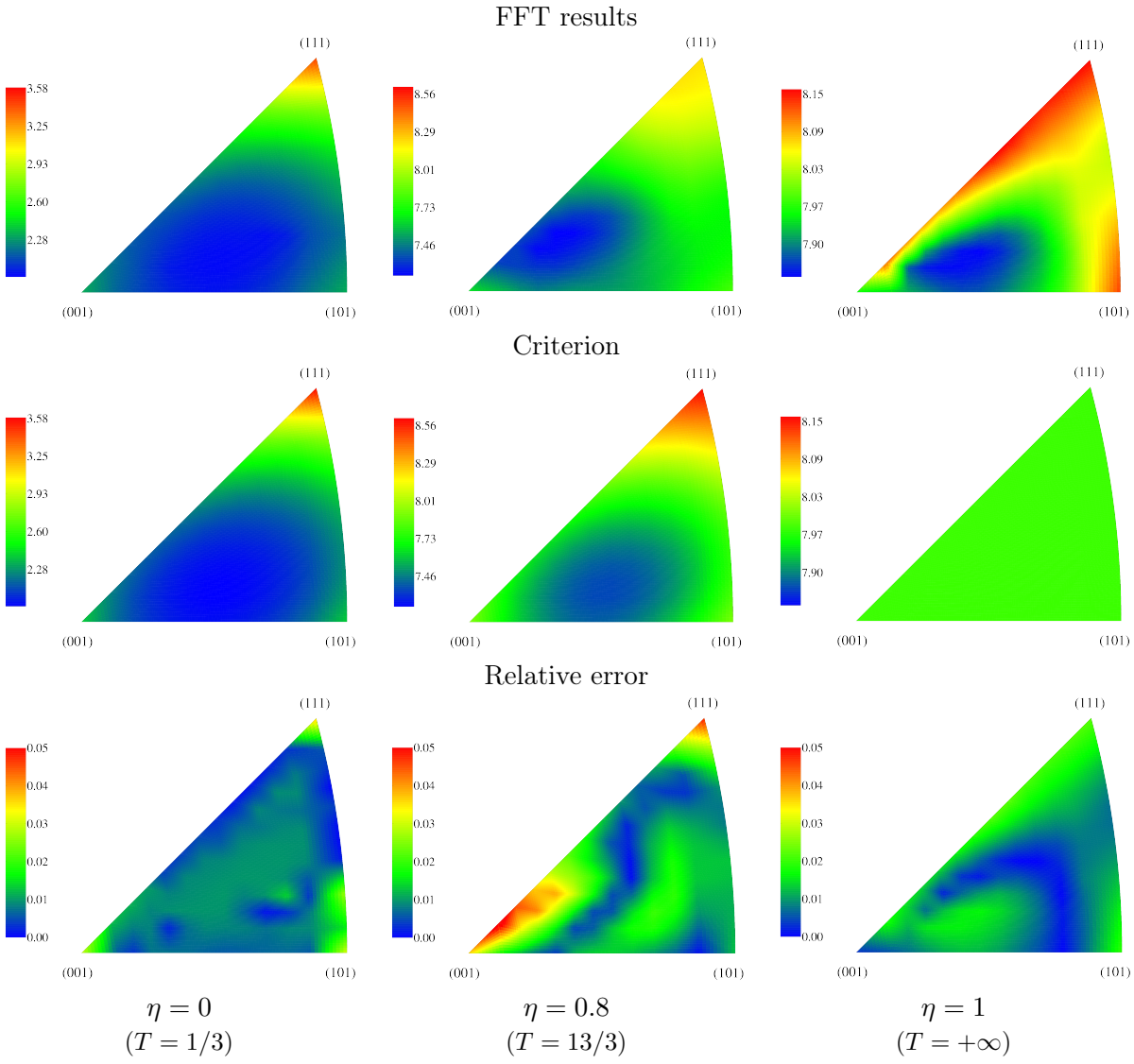

Figure 3: Inverse pole figure representation of the normalized yield stress Σ_I/τ^c of FCC crystals with 1% porosity subjected to an axisymmetric stress state

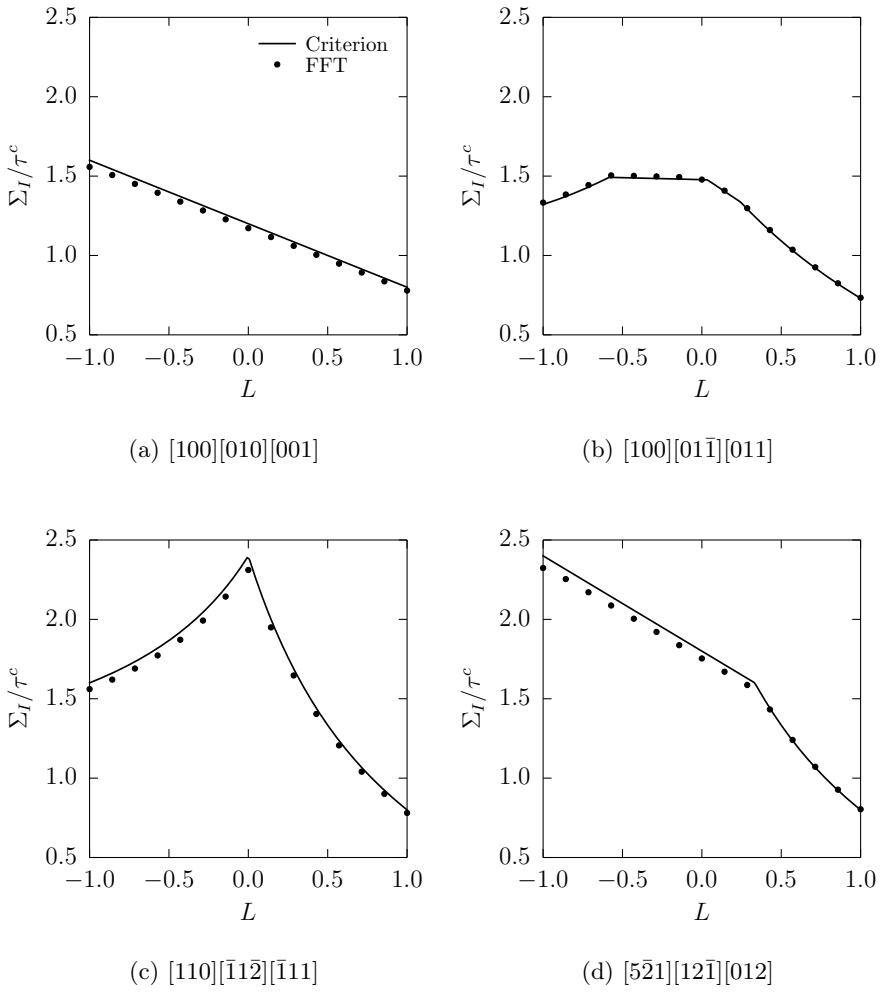

(a) [100][010][001]

(b) [100][01$\bar{1}$][011]

(c) [110][$\bar{1}$1$\bar{2}$][$\bar{1}$11]

(d) [5$\bar{2}$1][12$\bar{1}$][012]

Figure 4: Normalized yield stress Σ_I/τ^c of FCC crystals with 1% porosity for different orientations as a function of the Lode parameter L (Stress triaxiality $T = 0$)

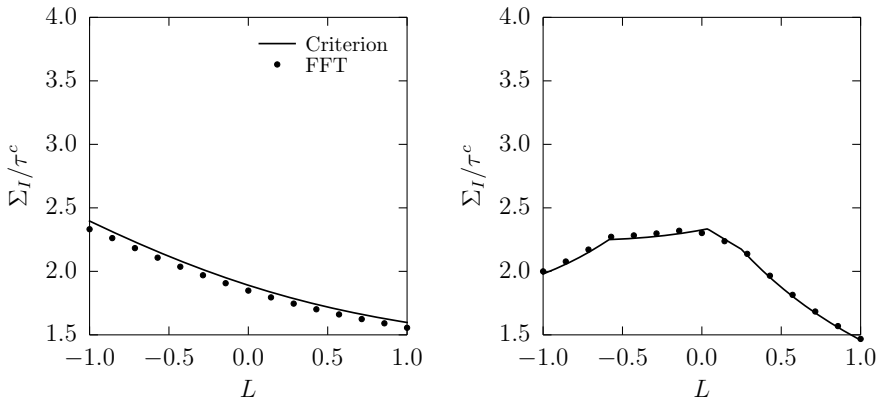

(a) [100][010][001]

(b) [100][01$\bar{1}$][011]

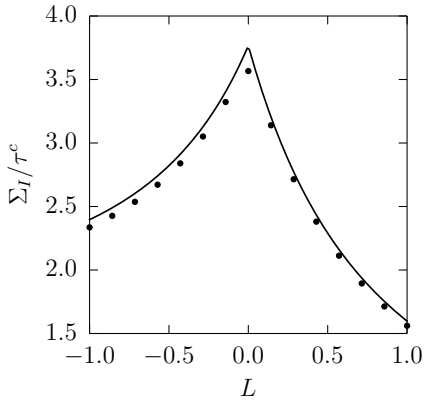

(c) [110][$\bar{1}$1$\bar{2}$][$\bar{1}$11]

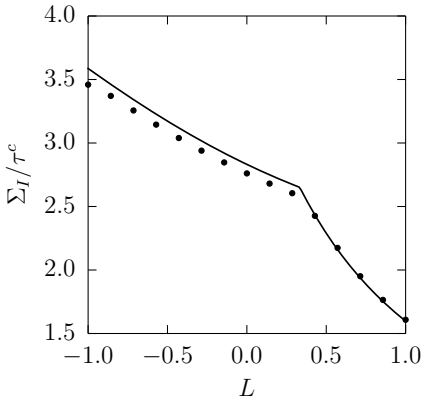

(d) [5$\bar{2}$1][12$\bar{1}$][012]

Figure 5: Normalized yield stress Σ_I/τ^c of FCC crystals with 1% porosity for different orientations as a function of the Lode parameter L (Stress triaxiality $T = 1/3$)

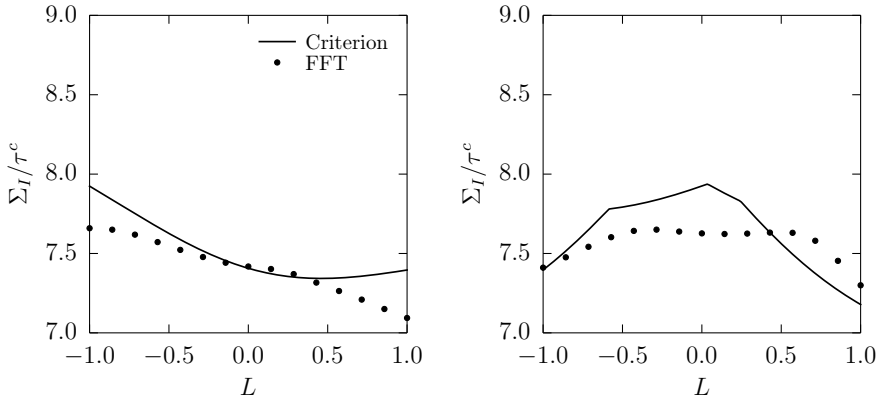

(a) [100][010][001]

(b) [100][01$\bar{1}$][011]

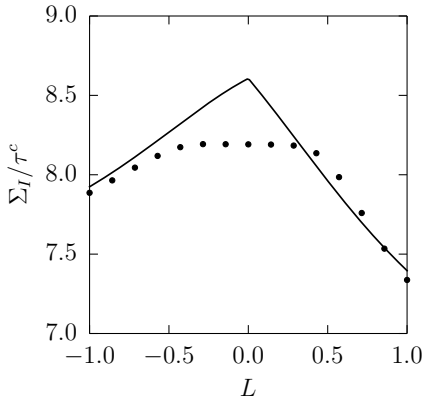

(c) [110][$\bar{1}$1$\bar{2}$][$\bar{1}$11]

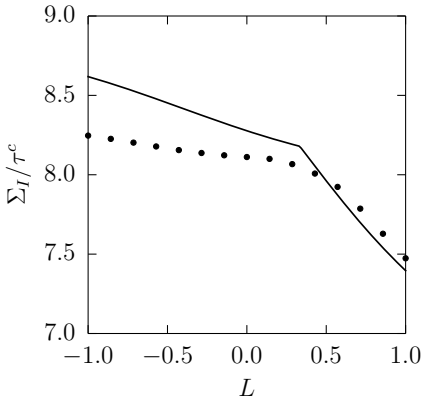

(d) [5$\bar{2}$1][12$\bar{1}$][012]

Figure 6: Normalized yield stress Σ_I/τ^c of FCC crystals with 1% porosity for different orientations as a function of the Lode parameter L (Stress triaxiality $T = 13/3$)

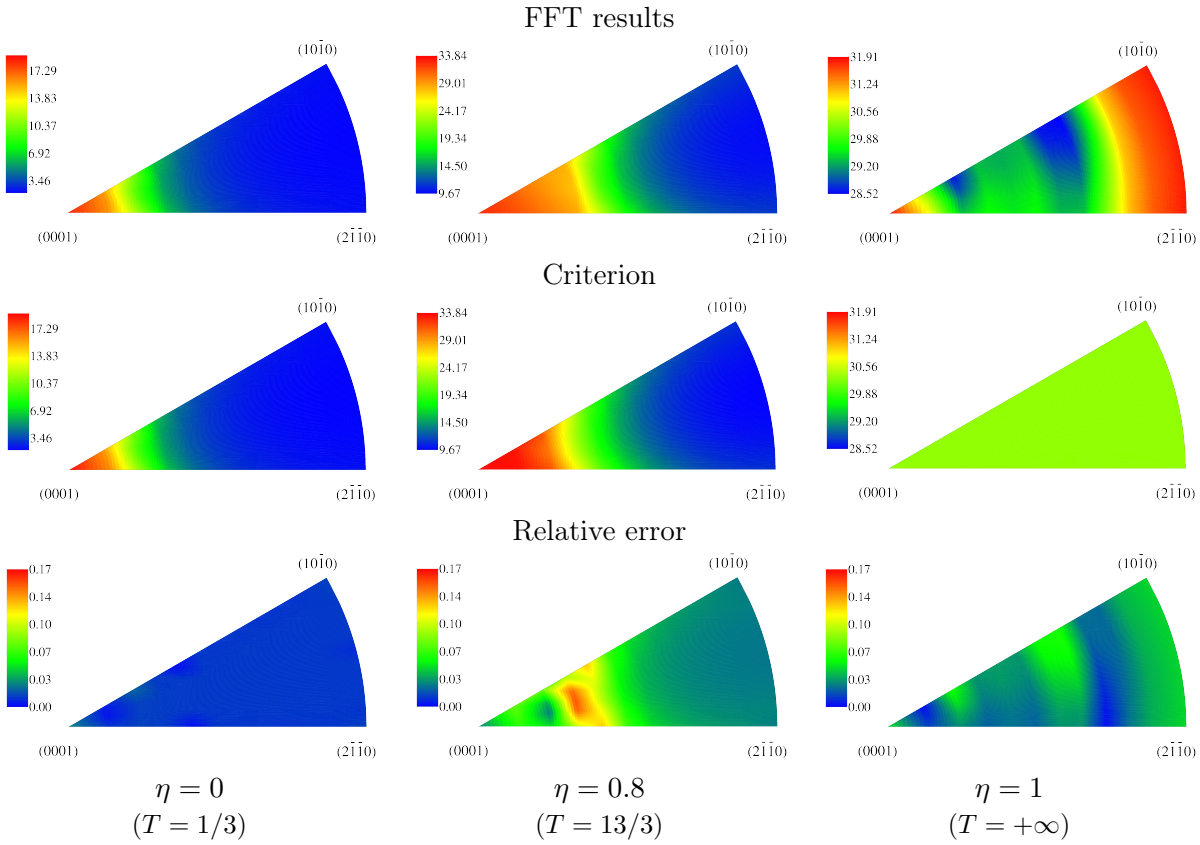

Figure 7: Inverse pole figure representation of the normalized yield stress $\Sigma_I/\tau^c_{Pr.}$ of Ti-like HCP crystals with 1% porosity subjected to an axisymmetric stress state.

For each crystalline structure, the fitting q parameter obtained is of the order of 2. Due to the strong plastic anisotropy, the yield stress of the voided crystals presents a distinct orientation dependence which is correctly reproduced by the criterion (Figures 7 and 8). Also, for the hydrostatic loading, the influence of the microstructural changes (see above) on the FFT numerical results is more important. This is consistent with the marked plastic anisotropy of the crystals. Besides, compared to the FCC structure, a notably higher hydrostatic yield stress is predicted (Taylor factor $\Sigma_I/\min(\tau^c) \sim 30$). This is due to the presence of "hard" directions for the plastic flow. In the limit of deficient crystals (i.e. lack of five independent slip systems), as evoked at the end of Section 2, the hydrostatic yield stress is infinite (i.e. the porous crystal is incompressible).

Globally, the approximate criterion leads to a worse agreement with the numerical results in the case of hexagonal crystals which present a marked plastic anisotropy. Such a trend was expected owing to the choice made for the trial velocity field which, for a hydrostatic loading, is only exact for an isotropic matrix. This point is clearly illustrated in Figure 9 which presents the FFT numerical prediction of the equivalent plastic strain field for FCC and HCP crystals, subjected to a hydrostatic loading, for a given macroscopic volume change $3E_m$. In the case of FCC crystals, the actual plastic strain field deviates from the isotropic one but, due to the cubic symmetry, the void growth remains spherical ($E_{\text{eq}} = 0$). On the contrary, zones with no plastic activity appear for HCP crystals due to the high plastic anisotropy. This results in a non spherical growth of the void ($E_{\text{eq}} \neq 0$). The difference between the patterns in

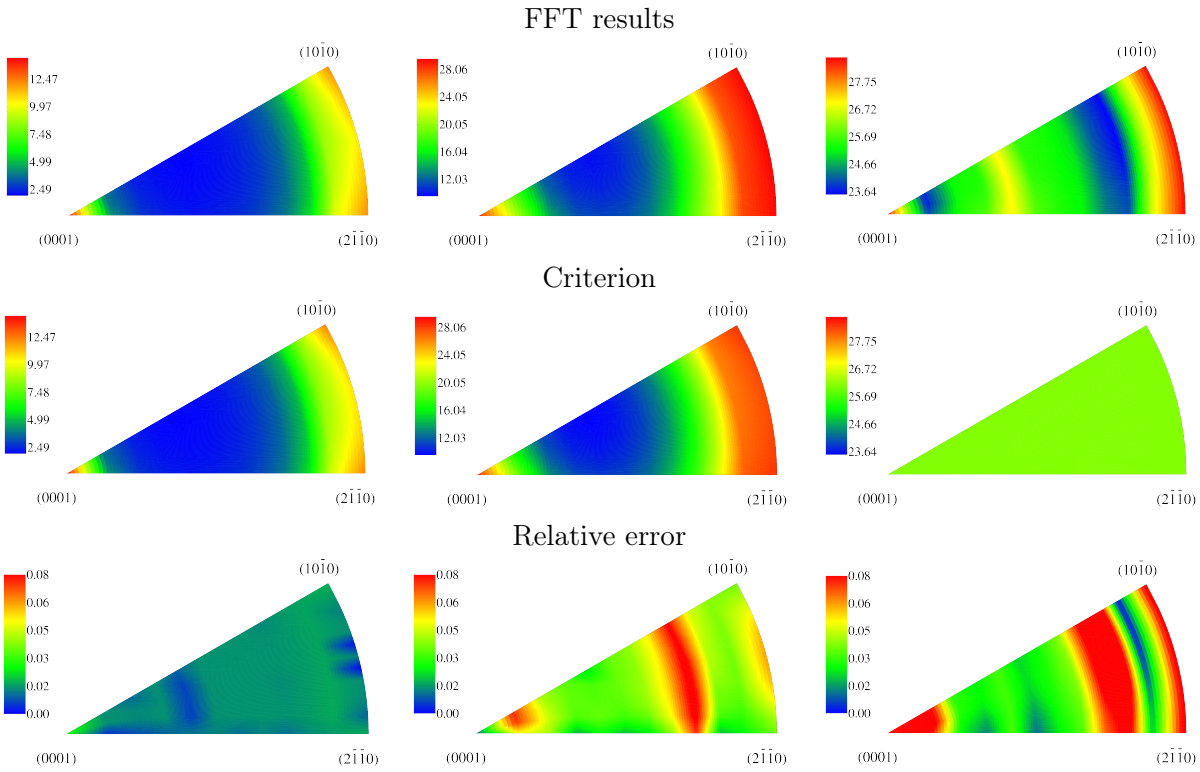

Figure 8: Inverse pole figure representation of the normalized yield stress $\Sigma_I/\tau^c_{Bas.}$ of Mg-like HCP crystals with 1% porosity subjected to an axisymmetric stress state.

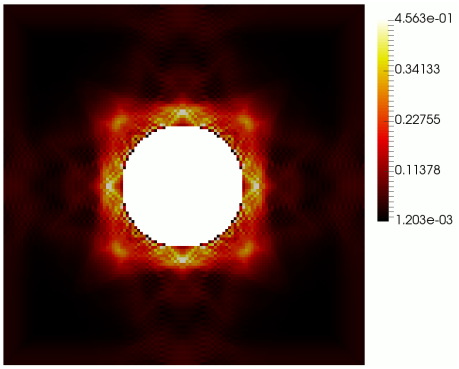

(a) FCC

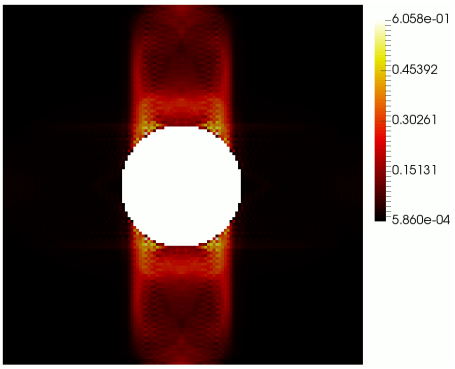

(b) $\mathrm{HCP_{Mg}}$

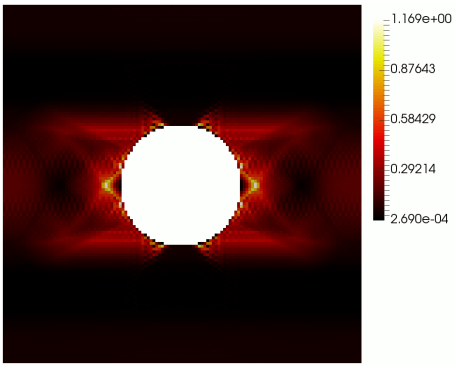

(c) $\mathrm{HCP_{Ti}}$

Figure 9: Equivalent plastic strain field $\boldsymbol{\varepsilon}^p_{\mathrm{eq}}$ for a macroscopic stress hydrostatic loading with different crystal anisotropies and a porosity of 2%. The overall mean strain is $E_m = 4.10^{-3}$. The plots corresponds to a planar cut at the middle of the cubic unit-cell. For the HCP crystals, the senar **c**-axis is vertical.

Figures 9b and 9c is due to the fact that the easy glide system differs (basal for the Mg-like crystal and prismatic for the Ti-like one). It must also be noted that, in the context of limit-analysis, we have used results from the usual approach which neglects a term of interaction between the deviatoric and the hydrostatic part of the strain rate test field. This issue has been studied by Leblond and Morin (2014) in the case of a von Mises matrix. However, the assumption of isotropy for the test field is expected to be the main explanation for the discrepancies.

4. Extension to hardenable porous crystals

By considering an associated flow rule, the proposed criterion (2.25) allows to describe the response of elastic-perfectly plastic porous crystals with fixed void shape and evolving porosity. To consider more general and realistic situations, we investigate the effects of the hardening within the proposed approach. More specifically, the case of isotropic hardening is considered.

4.1. General approach

It is proposed to extend the yield criterion by taking into account crystalline hardening. An approach similar to the one used by Leblond et al. (1995), for the case of an isotropic plastic matrix, is considered: we perform an approximate analysis of a hardenable rigid plastic crystalline hollow sphere subjected to a macroscopic prestrain $\mathbf{E}$. The macroscopic yield criterion is deduced by a kinematical limit analysis which consists in the following steps:

S1. Determine the local plastic strain $\boldsymbol{\varepsilon}^p(\mathbf{E},\mathbf{x})$ and the new geometry of the hollow sphere (i.e. overall domain $\Omega(\mathbf{E})$ and void domain $\omega(\mathbf{E})$).

S2. Deduce the evolution of the local polyhedral plastic domain (i.e. statically admissible stress space described by its set of vertices $\mathcal{A}(\boldsymbol{\varepsilon}^p(\mathbf{E},\mathbf{x}))$) induced by the plastic strain field.

S3. For an arbitrary macroscopic strain rate $\mathbf{D}$, calculate the global plastic dissipation

$$\Pi(\mathbf{E},\mathbf{D}) = \frac{1}{\Omega(\mathbf{E})} \inf_{\mathbf{d}\in\mathcal{K}(\mathbf{D},\mathbf{E})} \int_{\Omega(\mathbf{E})-\omega(\mathbf{E})} \sup_{\boldsymbol{\sigma}^*\in\mathcal{A}(\boldsymbol{\varepsilon}^p(\mathbf{E},\mathbf{x}))} \boldsymbol{\sigma}^* : \mathbf{d}(\mathbf{D},\mathbf{x})\ \mathrm{d}V \tag{4.1}$$

where $\mathcal{K}(\mathbf{D},\mathbf{E})$ is the set of kinematically admissible strain rate fields for the new geometry.

S4. Deduce the macroscopic yield surface with

$$\boldsymbol{\Sigma} = \frac{\partial\Pi(\mathbf{E},\mathbf{D})}{\partial\mathbf{D}}. \tag{4.2}$$

To obtain an approximate solution of the limit analysis problem, which cannot be solved exactly in general, the following assumptions are introduced:

A1. The shape change induced by $\mathbf{E}' = \mathrm{dev}(\mathbf{E})$ is neglected (i.e. the domain $\Omega(\mathbf{E})$ is a sphere).

A2. The local plastic strain field $\boldsymbol{\varepsilon}^p$ is estimated by the integration of the Rice-Tracey test field (2.14) between $t=0$ and $t=t_f$ with $\mathbf{D}=\mathbf{E}/t_f$. At time $t=t_f$, the plastic strain at radius $R=r(t_f)$ thus reads (Appendix B)

$$\boldsymbol{\varepsilon}^p(R) = \int_0^{t_f} \mathbf{d}\left(\mathbf{E}/T, r(t), t\right)\ \mathrm{d}t = \mathbf{E}' + \ln\frac{R}{\sqrt[3]{R^3+b^3-B^3}}\,\mathbf{d}_m \tag{4.3}$$

with b and B the initial and current outer radii of the sphere.
As a consequence of assumptions *A1* and *A2*, the studied cell remains a hollow sphere with current internal and external radii A and B.

A3. Use is also made of the Rice-Tracey velocity field (2.14) to obtain an upper bound of the global dissipation

$$\Pi(\mathbf{E},\mathbf{D}) = \frac{1}{\Omega(\mathbf{E})}\int_{\Omega(\mathbf{E})-\omega(\mathbf{E})} \sup_{\boldsymbol{\sigma}^*\in\mathcal{A}(\boldsymbol{\varepsilon}^p(\mathbf{E},\mathbf{x}))} \boldsymbol{\sigma}^* : \mathbf{d}(\mathbf{D},\mathbf{x})\ \mathrm{d}V \tag{4.4}$$

To avoid any confusion, it is pointed out that $\mathbf{E}$ (macroscopic prestrain) and $\mathbf{D}$ (macroscopic strain rate) are independent variables.

A4. The regularized macroscopic plastic yield function is expressible in the form

$$\mathcal{F}^{(n)}_{\mathrm{reg}}(\boldsymbol{\Sigma},\mathbf{E}) = \left(\sum_k \left(\frac{|\boldsymbol{\Sigma}:\boldsymbol{\mu}_k|}{\widetilde{\tau}^c_k(\mathbf{E})}\right)^n\right)^{\frac{2}{n}} + 2qP\cosh(\widetilde{\kappa}(\mathbf{E})\Sigma_m) - 1 - (qP)^2. \tag{4.5}$$

with P the current porosity. The functions $\widetilde{\tau}^c_k(\mathbf{E})$ and $\widetilde{\kappa}(\mathbf{E})$ are determined by considering, respectively, purely deviatoric ($\mathbf{D}=\mathbf{D}'$) and hydrostatic ($\mathbf{D}=D_m\mathbf{i}$) loadings.

4.2. Effective hardening functions $\widetilde{\tau}^c_k(\mathbf{E})$ and $\widetilde{\kappa}(\mathbf{E})$

• *Deviatoric strain rate loading:* By considering a deviatoric macroscopic strain rate $\mathbf{D}=\mathbf{D}'$, the global dissipation reads

$$\Pi(\mathbf{E},\mathbf{D}) \;=\; \frac{1}{\Omega(\mathbf{E})}\int_{\Omega(\mathbf{E})-\omega(\mathbf{E})} \max_{\boldsymbol{\sigma}^*\in\mathcal{A}(\boldsymbol{\varepsilon}^p(\mathbf{E},\mathbf{x}))} \boldsymbol{\sigma}^* : \mathbf{D}'\ \mathrm{d}V \tag{4.6}$$

Thus the macroscopic yield surface is given by

$$\boldsymbol{\Sigma} = \frac{\partial\Pi(\mathbf{E},\mathbf{D})}{\partial\mathbf{D}} = \frac{1}{\Omega(\mathbf{E})}\int_{\Omega(\mathbf{E})-\omega(\mathbf{E})} \operatorname*{argmax}_{\boldsymbol{\sigma}^*\in\mathcal{A}(\boldsymbol{\varepsilon}^p(\mathbf{E},\mathbf{x})} \boldsymbol{\sigma}^* : \mathbf{D}'\ \mathrm{d}V \tag{4.7}$$

By contrast with the perfectly plastic case, $\operatorname{argmax}(\boldsymbol{\sigma}^* : \mathbf{D}')$ generally varies with position vector $\mathbf{x}$ due to the heterogeneity of the hardening. By choosing $\mathbf{D}'=\boldsymbol{\mu}_k$, we have

$$\begin{aligned} |\boldsymbol{\Sigma}:\boldsymbol{\mu}_k| \;&=\; \frac{1}{\Omega(\mathbf{E})}\int_{\Omega(\mathbf{E})-\omega(\mathbf{E})} \left|\left(\operatorname*{argmax}_{\boldsymbol{\sigma}^*\in\mathcal{A}(\boldsymbol{\varepsilon}^p(\mathbf{E},\mathbf{x})} \boldsymbol{\sigma}^* : \boldsymbol{\mu}_k\right) : \boldsymbol{\mu}_k\right| \mathrm{d}V \\ &=\; (1-P)\,\langle\tau^c_k\rangle_{\Omega(\mathbf{E})-\omega(\mathbf{E})} \end{aligned} \tag{4.8}$$

With the proposed criterion (4.5), it follows that

$$\widetilde{\tau}^c_k(\mathbf{E}) = \langle\tau^c_k\rangle_{\Omega(\mathbf{E})-\omega(\mathbf{E})}\,. \tag{4.9}$$

Note that it has been assumed that the set of active slip systems does not change during hardening.

• *Hydrostatic strain rate loading:* For an hydrostatic macroscopic strain rate $\mathbf{D}=D_m\mathbf{i}$, the overall plastic dissipation reads

$$\Pi(\mathbf{E},\mathbf{D}) = \frac{3|D_m|}{4\pi}\int_{\Omega(\mathbf{E})-\omega(\mathbf{E})} \max_{\boldsymbol{\sigma}^*\in\mathcal{A}(\boldsymbol{\varepsilon}^p(\mathbf{E},\mathbf{x}))} \frac{\boldsymbol{\sigma}^* : \mathbf{d}_m}{R^3}\ \mathrm{d}V \tag{4.10}$$

and the mean yield stress is given by

$$\Sigma_m(\mathbf{E}) = \frac{1}{3}\frac{\partial \Pi(\mathbf{E},\mathbf{D})}{\partial D_m} = \frac{1}{4\pi}\int_{\Omega(\mathbf{E})-\omega(\mathbf{E})} \max_{\boldsymbol{\sigma}^* \in \mathcal{A}(\boldsymbol{\varepsilon}^p(\mathbf{E},\mathbf{x}))} \frac{\boldsymbol{\sigma}^* : \mathbf{d}_m}{R^3}\, \mathrm{d}V\ \mathrm{sgn}(D_m) \tag{4.11}$$

With the expression of the criterion (4.5), we get

$$\tilde{\kappa}(\mathbf{E}) = -\frac{\ln P}{\Sigma_m(\mathbf{E})}. \tag{4.12}$$

Hence, the estimation of the effective hardening functions requires the computation of the integrals (4.9) and (4.11) over the sphere volume. It is broached in the sequel for specific constitutive hardening laws. It can be noted that this approach, contrary to the one proposed by Ling et al. (2016), approximates the hardening by resorting to an estimation of the heterogeneity of the plastic strain field.

4.3. Constitutive hardening laws

We consider the evolution of the single crystal yield surface with plastic strain (i.e. increase of the critical resolved shear stresses τ_k^c). Following Mandel (1965) and Hill (1966), the hardening law takes the form

$$\dot{\tau_k^c} = \sum_{l=1}^{K} h_{kl}\dot{\gamma}_l \tag{4.13}$$

with $[h]$ the hardening matrix. In the case of linear hardening, a usual form is

$$h_{ij} = h_0(\delta_{ij} + q_l(1-\delta_{ij})) \tag{4.14}$$

where δ_{ij} is the kronecker symbol. h_0 and q_l are constant material parameters with $h_0 > 0$ and $q_l \geq 1$. h_0 represents the self hardening and $q_l h_0$ the latent hardening. The classical Taylor isotropic hardening rule corresponds to $q_l = 1$. Besides, nonlinear hardening is usually described, at the slip system scale, by Swift-type law (monotonic hardening) (see, for instance, Yerra et al., 2010)

$$\dot{\tau_k^c} = n_k \frac{\tau_k^0}{\Gamma_k^0}\left(\frac{\tau_k^c}{\tau_k^0}\right)^{\frac{n_k-1}{n_k}} \dot{\Gamma}_k \tag{4.15}$$

or Voce-type law (saturating hardening) (Sarma et al., 1998; Suquet et al., 2012)

$$\dot{\tau_k^c} = (\tau_k^\infty - \tau_k^c)\dot{\Gamma}_k. \tag{4.16}$$

$\dot{\Gamma}_k$ are the weighted sums of plastic slip rates on all the slip systems

$$\dot{\Gamma}_k = \sum_s a_{ks}\dot{\gamma}_s \tag{4.17}$$

τ_k^0 represents the initial critical shear stress on slip system k

$$\tau_k^0 = \tau_k^c(\Gamma_k = 0) \tag{4.18}$$

while τ_k^∞ is the stationary one in the Voce-type saturating hardening model. Γ_k^0, a_{ks} and n_k are positive hardening parameters (no units). Note also that a dislocation-based hardening law derived from the physical processes of storage and annihilation of dislocations during plastic deformation has been

proposed (Essmann and Mughrabi, 1979; Teodosiu et al., 1993; Tabourot et al., 1997). It describes a nonlinear evolution of the critical shear stresses with a stationary regime (saturation of the hardening). In the context of porous crystals, it has been recently used by Ling et al. (2016) for face-centred cubic materials. Linear and nonlinear hardening are considered in the sequel and an application of the derived model is made in the case of a Swift-type hardening law.

For a given plastic strain rate $\dot{\boldsymbol{\varepsilon}}^p$, the non-uniqueness of the set of plastic slip rates $\dot{\gamma}_k$ is a classical issue. Different iterative numerical algorithms for the discrimination of the plastic multipliers $\dot{\gamma}_k$ have been proposed (see, for instance, Anand and Kothari, 1996; Miehe and Schröder, 2001; Schmidt-Baldassari, 2003; Busso and Cailletaud, 2005). In the following, a pseudo-inverse method is used to determine an admissible set of plastic multipliers.

4.4. Approximate overall yield criterion for linear hardening

The effective critical shear stresses $\widetilde{\tau}_k^c(\mathbf{E})$ entering the criterion (4.5) may be written as

$$\widetilde{\tau}_k^c(\mathbf{E}) = \tau_k^0 + \frac{1}{\Omega(\mathbf{E}) - \omega(\boldsymbol{E})} \int_{\Omega(\mathbf{E})-\omega(\mathbf{E})} \Delta\tau_k^c(\boldsymbol{\varepsilon}^p(\mathbf{E},\mathbf{x}))\,\mathrm{d}V \tag{4.19}$$

with $\tau_k^0 = \tau_k^c(\mathbf{E}=\mathbf{0})$. The pointwise heterogeneity of the plastic strain field $\boldsymbol{\varepsilon}^p$ and its dependence on $\mathbf{E}$ make it difficult to derive an analytical expression for the increment of the local critical shear stresses $\Delta\tau_k^c(\boldsymbol{\varepsilon}^p(\mathbf{E},\mathbf{x}))$. Besides, the numerical estimate of (4.19) must be performed for each macroscopic prestrain $\mathbf{E}$. Albeit feasible, such a model is quite computationally expensive. To circumvent this issue, the local hardening due to the plastic strain $\boldsymbol{\varepsilon}^p(\mathbf{E},\mathbf{x})$ is approximated by the sum of the hardenings due to the successive plastic strains $\mathbf{E}'$ and $\mathbf{d}_m \ln \frac{R}{\sqrt[3]{R^3+b^3-B^3}}$. That is

$$\Delta\tau_k^c(\boldsymbol{\varepsilon}^p(\mathbf{E},\mathbf{x})) \simeq \Delta\tau_k^c(\mathbf{E}') + \Delta\tau_k^c(\mathbf{d}_m \ln \frac{R}{\sqrt[3]{R^3+b^3-B^3}}). \tag{4.20}$$

By using the linearity of the constitutive hardening law (relations (4.13) and (4.14)),

$$\Delta\tau_k^c(\mathbf{d}_m \ln \frac{R}{\sqrt[3]{R^3+b^3-B^3}}) = \ln\left(\frac{R}{\sqrt[3]{R^3+b^3-B^3}}\right)\,\Delta\tau_k^c(\mathbf{d}_m) \tag{4.21}$$

the effective critical shear stresses $\widetilde{\tau}_k^c(\mathbf{E})$ can be expressed as

$$\widetilde{\tau}_k^c(\mathbf{E}) = \tau_k^0 + \Delta\tau_k^c(\mathbf{E}') + \chi(E_m) H_k \tag{4.22}$$

with

$$H_k = \int_{R=1} \Delta\tau_k^c(\mathbf{d}_m)\,\mathrm{d}S \tag{4.23}$$

and

$$\chi(E_m) = \frac{1}{\Omega(\mathbf{E}) - \omega(\boldsymbol{E})} \int_A^B \ln\left(\frac{R}{\sqrt[3]{R^3+b^3-B^3}}\right) R^2\,\mathrm{d}R. \tag{4.24}$$

By using the change of variables $R = Bu$ and the relation $b^3 = B^3 e^{-3E_m}$, by definition of E_m, $\chi(E_m)$ takes the simpler form

$$\chi(E_m) = \frac{3}{4\pi(1-P)} \int_{P^{\frac{1}{3}}}^1 \ln \frac{u}{\sqrt[3]{u^3 + e^{-3E_m} - 1}} u^2\,\mathrm{d}u. \tag{4.25}$$

Besides, the mean yield stress $\Sigma_m(\mathbf{E})$ reads

$$\Sigma_m(\mathbf{E}) = \frac{1}{4\pi} \int_{\Omega(\mathbf{E})-\omega(\mathbf{E})} \frac{1}{R^3} \max_{\boldsymbol{\sigma}^* \in \mathcal{A}(\boldsymbol{\varepsilon}^p(\mathbf{E},\mathbf{x}))} \boldsymbol{\sigma}^* : \mathbf{d}_m \, \mathrm{d}V \, \mathrm{sgn}(D_m). \tag{4.26}$$

By using the expression of the plastic strain rate $\mathbf{d}_m$,

$$\mathbf{d}_m = \sum_k \dot{\gamma}_k^{\mathbf{d}_m} \boldsymbol{\mu}_k, \tag{4.27}$$

it follows that

$$\Sigma_m(\mathbf{E}) = \frac{1}{4\pi} \int_{\Omega(\mathbf{E})-\omega(\mathbf{E})} \frac{1}{R^3} \sum_k \dot{\gamma}_k^{\mathbf{d}_m} \, \tau_k^c(\boldsymbol{\varepsilon}^p(\mathbf{E},\mathbf{x})) \, \mathrm{d}V \, \mathrm{sgn}(D_m). \tag{4.28}$$

By using the approximation (4.20) and the linearity of the hardening law, the mean yield stress is expressible in the form

$$\Sigma_m(\mathbf{E}) = -\frac{\ln P}{12\pi} \left(\sum_k I_{\gamma_k} \, (\tau_k^0 + \Delta\tau_k^c(\mathbf{E}')) + I_\Delta \, \beta(E_m) \right) \mathrm{sgn}(D_m) \tag{4.29}$$

with

$$I_{\gamma_k} = \int_{R=1} \dot{\gamma}_k^{\mathbf{d}_m} \, \mathrm{d}S, \quad I_\Delta = \sum_k \int_{R=1} \dot{\gamma}_k^{\mathbf{d}_m} \Delta\tau_k^c(\mathbf{d}_m) \, \mathrm{d}S \tag{4.30}$$

and

$$\beta(E_m) = -\frac{3}{\ln P} \int_A^B \ln \left(\frac{R}{\sqrt[3]{R^3 + b^3 - B^3}} \right) \frac{\mathrm{d}R}{R}. \tag{4.31}$$

By using the change of variables $R = Bu$, the function $\beta(E_m)$ also reads

$$\beta(E_m) = -\frac{3}{\ln P} \int_{P^{\frac{1}{3}}}^1 \ln \left(\frac{u}{\sqrt[3]{u^3 + e^{-3E_m} - 1}} \right) \frac{\mathrm{d}u}{u}. \tag{4.32}$$

In the absence of hardening, it can be checked that the non vanishing integral term in (4.29), $\sum_k I_{\gamma_k} \tau_k^0$, corresponds to the integral I_Π (2.22) which appears in the criterion for perfect plasticity. The estimation of the effective hardening parameters has thus been reduced to the computations of three integrals on the unit sphere (H_k, I_{γ_k} and I_Δ), which do not depend on $\mathbf{E}$, and two integral functions (β and χ), purely geometrical, which only depend on the macroscopic mean strain E_m.

4.5. Approximate overall yield criterion for nonlinear hardening

In the case of nonlinear hardening, it is necessary to add a supplementary approximation (i.e. linearization of the hardening law) to make use of the previously derived semi-analytical criterion. Hereafter, we consider the particular case of an isotropic Swift-type hardening at the slip system scale (4.15) which also reads

$$\dot{\tau}^c(\mathbf{x}) = n \frac{\tau^0}{\Gamma^0} \left(1 + \frac{\Gamma(\mathbf{x})}{\Gamma^0} \right)^{n-1} \dot{\Gamma}(\mathbf{x}), \quad \dot{\Gamma} = \sum_k \dot{\gamma}_k, \quad n \in [0;1]. \tag{4.33}$$

$n = 0$ corresponds to perfect plasticity while $n = 1$ describes a linear hardening. The linearized form of (4.33) reads

$$\dot{\tau}^c(\mathbf{x}) \simeq n \frac{\tau^0}{\Gamma^0} \left(1 + \frac{\Gamma_{\mathrm{ref}}}{\Gamma^0} \right)^{n-1} \dot{\Gamma}(\mathbf{x}) \tag{4.34}$$

with Γ_{ref} a reference cumulative plastic slip. Two definitions of Γ_{ref} will be considered, namely a *first moment (average)* approximation

$$\Gamma_{\text{ref}} = \langle \Gamma \rangle_{\Omega(\mathbf{E})-\omega(\mathbf{E})} \tag{4.35}$$

and a *second moment* approximation

$$\Gamma_{\text{ref}} = \sqrt{\langle \Gamma^2 \rangle_{\Omega(\mathbf{E})-\omega(\mathbf{E})}}. \tag{4.36}$$

Considering the nonlinearity of the hardening law and the heterogeneity of the cumulative plastic slip within the hollow sphere, the latter approximation yields a better approximation of $\langle \tau_k^c \rangle_{\Omega(\mathbf{E})-\omega(\mathbf{E})}$.

4.6. Assessment with respect to FE computations

4.6.1. Approximate models

Based on the approximate yield function (4.5) with hardening functions (4.9) and (4.12), a constitutive macroscopic elastoplastic model has been derived by using the normality rule for the plastic flow and the Hooke's law of the single crystal. It is pointed out that the influence of the porosity on the overall elastic behaviour is neglected. Thus, the elastoplastic homogenization problem is being fully decoupled. These approximations are justified by the low initial porosity value considered. The proposed model has been compared qualitatively to finite strain FE results for BCC single crystals (Yerra et al., 2010). It must be noted that the FE computations have been performed with a viscoplastic flow rule. However, the strain-rate sensitivity coefficient m being very low ($m = 0.01$), the local behaviour is almost rate-independent.

Different levels of approximations are considered for the evaluation of the integrals defining the effective hardening parameters $\widetilde{\tau}_k^c(\mathbf{E})$ (4.9) and $\tilde{\kappa}(\mathbf{E})$ (4.12). The approximation based on the full numerical computation with the nonlinear hardening law is called FNLH (Full Non Linear Hardening) and the assumption of additive decomposition of the hardening (4.20) is called DNLH (Decomposed Non Linear Hardening). Based on this decomposition, the additional use of the linearization of the hardening law (4.34) defines two approximations DLH1 and DLH2 (Decomposed Linearized Hardening) using respectively the average and the second moment of the cumulative plastic slip to define the reference value Γ_{ref}.

4.6.2. Results

Tests have been performed for various orientations of the loading axis with respect to the crystal reference frame. The simulations are performed by imposing the strain rate component along the loading axis and the overall stress triaxiality. The figure 10 shows the overall stress-strain response as well as the porosity evolution predicted by the approximate model FNLH and the FE computations of Yerra et al. (2010). It can be observed that the orientation dependence of the behaviour is on the whole correctly described with a higher yield stress and void growth rate for the [110] orientation. For high stress triaxiality ($T = 3$), although the comparison is somewhat less good, it must be remarked that the crossing of the stress-strain curves of the orientations [110] and [111] after the peak stress is still correctly described.

Finally, the predictions of the overall stress-strain response with the different approximate models introduced has been compared to the FE results. The Figure 11 illustrates the main trends obtained. The models using a linearization of the hardening law leads as a whole to poor estimates. Nonetheless, it is noted that the second moment approximation of the reference cumulative plastic slip always give better results, as expected because of the plastic strain heterogeneity.

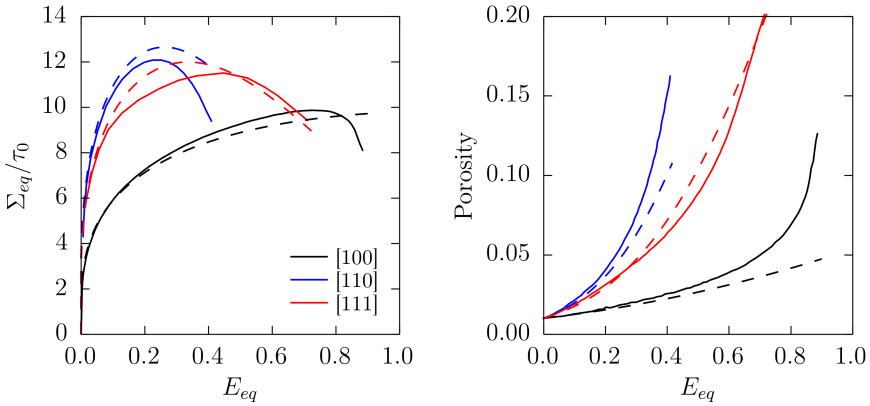

(a) Stress triaxiality $T = 1$

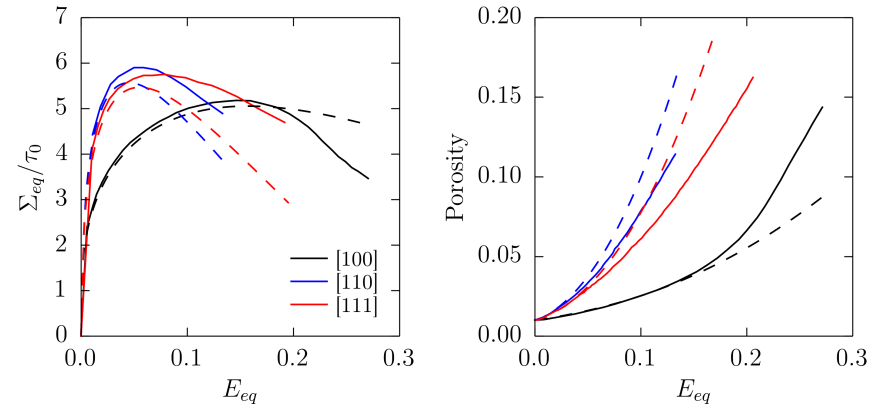

(b) Stress triaxiality $T = 3$

Figure 10: Overall stress-strain response and porosity evolution for BCC crystals with different orientations of the loading axis with respect to the crystalline reference frame. The hardening exponent is $n = 0.3$ (solid lines: FE results (Yerra et al., 2010); dashed lines: FNLH approximate model).

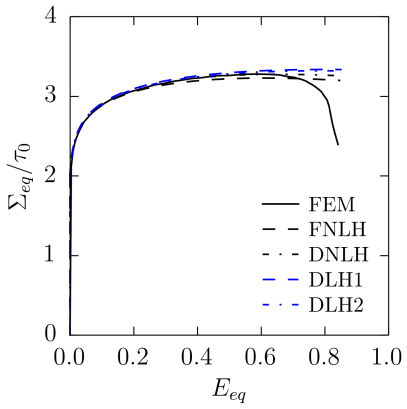

(a) [100], $T = 1$, $n = 0.1$

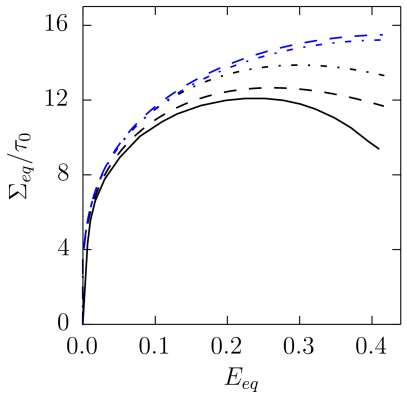

(b) [110], $T = 1$, $n = 0.3$

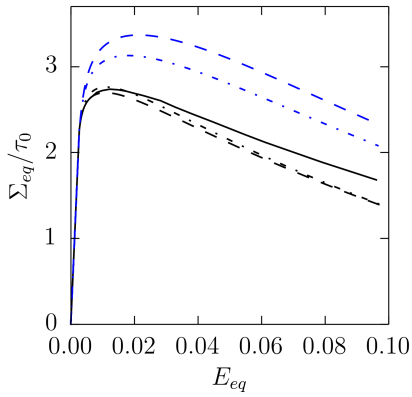

(c) [110], $T = 3$, $n = 0.1$

Figure 11: Comparison of the different approximate models (dashed lines) with the FE results of Yerra et al. (2010) (solid lines) for different crystalline orientations, stress triaxialities and hardening exponent.

5. Conclusion

This work, based on the kinematic limit analysis of a hollow sphere and unit-cell full-field computations, is a contribution to the understanding of the plastic behaviour of porous crystals . The approximate yield criterion proposed by Paux et al. (2015) has been extended to consider an arbitrary plastic anisotropy as well as the strain hardening at the slip system scale. Results have been reported for FCC and HCP crystals with different families of easy-glide systems. It is observed that the accuracy of the criterion decreases when the plastic anisotropy increases. However, a correct qualitative description of the orientation-dependent yield stress is obtained for finite stress triaxiality. Besides, the dependence of the hydrostatic yield stress with the plastic anisotropy (i.e. ratios of the critical shear stresses) is well predicted. In this context, it has also been emphasized that the incompressibility of porous single crystals, previously reported by Mbiakop et al. (2015a), is due to their deficiency of slip systems (i.e. infinite plastic anisotropy).

An extension of the criterion to hardenable crystals has been derived by considering the approach originally proposed by Leblond et al. (1995) for a von Mises material. It allows to consider, approximately, the spatial heterogeneity of the strain hardening to define effective hardening parameters. Different approximations have been proposed for linear and nonlinear (isotropic) hardening. A constitutive model has been derived based on this criterion and it has been assessed by comparison with unit-cell FE results on BCC crystals (Yerra et al., 2010). A good qualitative agreement, with in particular the correct description of the dependence on the crystal orientation, is obtained. Further developments are required to take into account the evolution of the void shape, which can be significant at low stress triaxiality, as well as the lattice rotation of the crystal during the plastic deformation.

Appendix A. Incompressibility of deficient porous crystals

We aim to prove that a hollow sphere consituted of a single crystal lacking five independent slip systems is incompressible when subjected to homogeneous strain rate boundary conditions. In the case of a macroscopic volume change rate, the boundary conditions read

$$\mathbf{v} = \mathbf{d}.\mathbf{x} = D_m\,\mathbf{x}, \quad \forall \mathbf{x} \in \partial\Omega\ (\mathbf{x} = b\,\mathbf{e}_r) \tag{A.1}$$

As the velocity field $\mathbf{v}$ is known on the boundary $\partial\Omega$, its partial derivatives in the tangent plane are known. They define a part of the strain rate tensor $\mathbf{d}$ at the boundary surface. In the sequel, it is shown that a deficient single crystal cannot accommodate this part of the strain rate.

Surface strain rate: Let $\mathcal{B}_\mathbf{p} = (\mathbf{x_p}, \mathbf{y_p}, \mathbf{n_p})$ an orthonormal basis with $\mathbf{n_p}$ the unit outer normal at point $\mathbf{p} \in \partial\Omega$. The strain rate at point $\mathbf{p}$ reads

$$\mathbf{d}(\mathbf{p}) = \frac{1}{2}\left(\boldsymbol{\nabla}\mathbf{v} + \boldsymbol{\nabla}\mathbf{v}^{\mathrm{T}}\right) = D_m \begin{pmatrix} 1 & 0 & \frac{1}{2}\frac{\partial v_x}{\partial z} \\ 0 & 1 & \frac{1}{2}\frac{\partial v_y}{\partial z} \\ \frac{1}{2}\frac{\partial v_x}{\partial z} & \frac{1}{2}\frac{\partial v_y}{\partial z} & -2 \end{pmatrix}_{\mathcal{B}_\mathbf{p}} \tag{A.2}$$

with unknown gradient components $\partial v_x/\partial z$ and $\partial v_y/\partial z$.

"Forbidden strain rate": For crystals lacking five independent slip systems, there is a "forbidden" deviatoric strain rate $\mathbf{d}_0$ such that, for all admissible strain rate $\mathbf{d}$, $\mathbf{d} : \mathbf{d}_0 = 0$ (Figure A.1). There is a basis

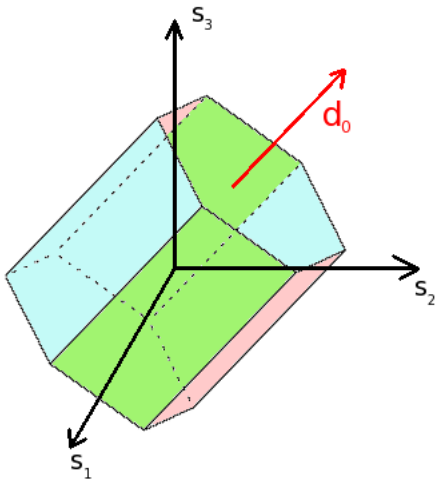

Figure A.1: Schematic illustration of the yield surface of a deficient crystal in the deviatoric eigenbasis (s_1, s_2, s_3). The space of admissible stresses (i.e. plastic domain) is defined by the different slip systems (in pink, green and blue). As there is not enough independent slip systems, the yield surface is not closed in the deviatoric space. $\mathbf{d}_0$ represents the "forbidden" strain rate direction.

$\mathcal{B}_0 = (\mathbf{x}_0, \mathbf{y}_0, \mathbf{z}_0)$ such that the strain rate $\mathbf{d}_0$ reads

$$\mathbf{d}_0 = \begin{pmatrix} a & 0 & 0 \\ 0 & b & 0 \\ 0 & 0 & c \end{pmatrix}_{\mathcal{B}_0} \tag{A.3}$$

with $(a, b, c) \neq (0, 0, 0)$ and $a + b + c = 0$ since $\mathbf{d}_0$ is deviatoric. Let's consider two specific points $\mathbf{p}_1$ and $\mathbf{p}_2$ on the surface $\partial\Omega$ such that $\mathbf{n}_{\mathbf{p}_1} = \mathbf{z_0}$ and $\mathbf{n}_{\mathbf{p}_2} = \mathbf{y_0}$ (Figure A.2). The condition $\mathbf{d}(\mathbf{p}) : \mathbf{d}_0 = 0$ gives, respectively, at points $\mathbf{p}_1$ and $\mathbf{p}_2$,

$$\begin{cases} a + b - 2c = 0, \\ a - 2b + c = 0. \end{cases} \tag{A.4}$$

Together with the incompressibility condition $(a + b + c = 0)$, the only solution for (a, b, c) is $(0, 0, 0)$, which is excluded. Thus, there is no solution to the problem. This implies that the single crystal cannot accomodate a macroscopic volume change with homogeneous strain rate boundary conditions.

Two points are worth emphasizing concerning this proof:

- It can be extended to any domain with smooth boundary under the same type of boundary conditions.
- The inner properties are not involved in the proof. The result thus holds whatever the content of the single crystal sphere. In particular, a hollow single crystal sphere deficient in independent slip systems remains incompressible whatever the distribution of the porosity.

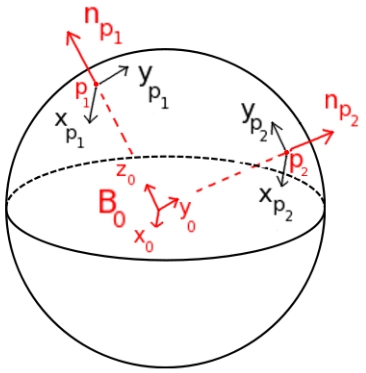

Figure A.2: Representation of the different basis $\mathcal{B}_0$, $\mathcal{B}_{\mathbf{p}_1}$ and $\mathcal{B}_{\mathbf{p}_2}$ defined on the outer surface $\partial\Omega$ of the sphere.

Appendix B. Plastic strain field and porosity evolution

For $t \in [0; t_f]$, it is assumed that (i) the cell remains spherical and (ii) the strain rate at a material point with radius $r(t)$ is of the form (2.14)

$$\mathbf{d}(r(t), t) = \frac{1}{t_f}\,\mathbf{E}' + \frac{\dot{b}(t)\,b(t)^2}{r(t)^3}\mathbf{d}_m. \tag{B.1}$$

The macroscopic strain at time t_f is $\mathbf{E} = \mathbf{E}' + E_m\mathbf{i}$ with E_m the macroscopic mean strain defined by

$$E_m = \int_0^{t_f} \frac{\dot{b}(t)}{b(t)}\,\mathrm{d}t. \tag{B.2}$$

The plastic strain reads

$$\boldsymbol{\varepsilon}^p(R) = \int_0^{t_f} \mathbf{d}(r(t), t)\,\mathrm{d}t = \mathbf{E}' + \int_0^{t_f} \frac{\dot{b}(t)\,b(t)^2}{r(t)^3}\,\mathrm{d}t\,\mathbf{d}_m. \tag{B.3}$$

Besides, the evolution of the radius $r(t)$ is

$$\dot{r}(t) = \dot{b}(t)\left(\frac{b(t)}{r(t)}\right)^2. \tag{B.4}$$

Consequently,

$$\int_0^{t_f} \frac{\dot{b}(t)b(t)^2}{r(t)^3}\,\mathrm{d}t = \int_0^{t_f} \frac{\dot{r}(t)}{r(t)}\,\mathrm{d}t = \ln\frac{R}{r_0} \tag{B.5}$$

with r_0 and R the initial and current radii. Let b and B (a and A) the initial and current outer (inner) radii of the sphere. Since the solid phase is incompressible

$$b^3 - B^3 = a^3 - A^3 = r_0^3 - R^3 \tag{B.6}$$

and the plastic strain rate finally reads

$$\boldsymbol{\varepsilon}^p(R) = \mathbf{E}' + \ln\frac{R}{\sqrt[3]{R^3 + b^3 - B^3}}\,\mathbf{d}_m. \tag{B.7}$$

From the definition of the macroscopic mean strain E_m (B.2), it follows that $B^3 = b^3\,\mathrm{e}^{3E_m}$. By taking into account the incompressibility of the matrix, the current porosity P (at time t_f) is thus expressible as (Leblond et al., 1995)

$$P = \frac{A^3}{B^3} = \frac{a^3 + (\mathrm{e}^{3E_m} - 1)\,b^3}{\mathrm{e}^{3E_m}\,b^3} = 1 + \frac{1}{\mathrm{e}^{3E_m}}(p_0 - 1) \tag{B.8}$$

where $p_0 = (a^3/b^3)$ is the initial porosity.

References

Agnew, S.R., Brown, D.W., Tomé, C.N., 2006. Validating a polycrystal model for the elastoplastic response of magnesium alloy AZ31 using in situ neutron diffraction. Acta Mater. 54, 4841–4852.

Anand, L., Kothari, M., 1996. A computational procedure for rate-independent crystal plasticity. J. Mech. Phys. Solids 44, 525–558.

Arminjon, M., 1991. A regular form of the Schmid law. Application to the ambiguity problem. Texture Microstruct. 14-18, 1121–1128.

Belkhabbaz, A., Bacroix, B., Brenner, R., 2015. Investigation of the elastoplastic behavior of FCC polycrytals using a FFT numerical scheme. Ro. J. Tech. Sci. - Appl. Mech. 60.

Belkhabbaz, A., Brenner, R., Rupin, N., Bacroix, B., Fonseca, J., 2011. Prediction of the overall behavior of a 3D microstructure of austenitic steel by using FFT numerical scheme. Procedia Engineering 10, 1883–1888.

Benzerga, A.A., Besson, J., 2001. Plastic potentials for anisotropic porous solids. Eur. J. Mech. A/Solids 20, 397–434.

Bishop, J.F.W., Hill, R., 1951. A theoretical derivation of the plastic properties of a polycrystalline face-centred metal. Phil. Mag. 42, 1298–1307.

de Botton, G., Ponte Castañeda, P., 1995. Variational estimates for the creep behaviour of polycrystals. Proc. R. Soc. Lond. A448, 121–142.

Brenner, R., Lebensohn, R.A., Castelnau, O., 2009. Elastic anisotropy and yield surface estimates of polycrystals. Int. J. Solids Struct. 46, 3018–3026.

Brisard, S., Dormieux, L., 2010. FFT-based methods for the mechanics of composites: A general variational framework. Comput. Mater. Sci. , 663–671.

Busso, E.P., Cailletaud, G., 2005. On the selection of active slip systems in crystal plasticity. Int. J. Plasticity 21, 2212–2231.

Crépin, J., Bretheau, T., Caldemaison, D., 1996. Cavity growth and rupture of β-treated zirconium: a crystallographic model. Acta mater. 44, 4927–4935.

Danas, K., Aravas, N., 2012. Numerical modeling of elasto-plastic porous materials with void shape effects at finite deformations. Composites: Part B 43, 2544–2559.

Essmann, U., Mughrabi, H., 1979. Annihilation of dislocations during tensile and cyclic deformation and limits of dislocation densities. Phil. Mag. A 40, 731–756.

Eyre, D.J., Milton, G.W., 1999. A fast numerical scheme for computing the response of composites using grid refinement. Journal of Physique III 6, 41–47.

Fundenberger, J.J., Philippe, M.J., Wagner, F., Esling, C., 1997. Modelling and prediction of mechanical properties for materials with hexagonal symmetry zinc, titanium and zirconium alloys. Acta Mater. 45, 4041–4055.

Gambin, W., 1992. Refined analysis of elastic-plastic crystals. Int. J. Solids Struct. 29, 2013–2021.

Gan, Y.X., Kysar, W., Morse, T.L., 2006. Cylindrical void in a rigid-ideally plastic single crystal II: Experiments and simulations. Int. J. Plast. 22, 39–72.

Groves, G.W., Kelly, A., 1963. Independent slip systems in crystals. Phil. Mag. 8, 877–887.

Han, X., Besson, J., Forest, S., Tanguy, B., Bugat, S., 2013. A yield function for single crystals containing voids. Int. J. Solids Struct. 50, 2115–2131.

Hill, R., 1948. A theory of the yielding and plastic flow of anisotropic metals. Proc. R. Soc. Lond. A193, 281–297.

Hill, R., 1950. The mathematical theory of plasticity. Oxford University Press.

Hill, R., 1966. Generalized constitutive relations for incremental deformation of metal crystals by multislip. J. Mech. Phys. Solids 14, 95–102.

Kocks, U.F., Canova, G.R., Jonas, J.J., 1983. Yield vectors in f.c.c. crystals. Acta metall. 31, 1243–1252.

Lebensohn, R.A., 2001. N-site modeling of a 3D viscoplastic polycrystal using fast fourier transform. Acta Mater. 49, 2723–2737.

Leblond, J.B., Morin, L., 2014. Gurson's criterion and its derivation revisited. J. Appl. Mech. - Trans. ASME 81, 051012.

Leblond, J.B., Perrin, G., Devaux, J., 1995. An improved Gurson-type model for hardenable ductile metals. Eur. J. Mech. A/Solids 14, 499–527.

Ling, C., Besson, J., Forest, S., Tanguy, B., Latourte, F., Bosso, E., 2016. An elastoviscoplastic model for porous single crystals at finite strains and its assessment based on unit cell simulations. Int. J. Plasticity 84, 58–87.

Mandel, J., 1965. Généralisation de la théorie de plasticité de W. T. Koiter. Int. J. Solids Struct. 1, 273–295.

Mbiakop, A., Constantinescu, A., Danas, K., 2015a. An analytical model for porous single crystals with ellipsoidal voids. J. Mech. Phys. Solids 84, 436–467.

Mbiakop, A., Constantinescu, A., Danas, K., 2015b. A model for porous single crystals with cylindrical voids of elliptical cross-section. Int. J. Solids Struct. 64-65, 100–119.

Michel, J.C., Moulinec, H., Suquet, P., 2001. A computational scheme for linear and non-linear composites with arbitrary phase contrast. Int. J. Numer. Meth. Engng 52, 139–160.

Miehe, C., Schröder, J., 2001. A comparative study of stress update algorithms for rate-independent and rate-dependent crystal plasticity. Int. J. Num. Meth. Engng 50, 273–298.

Monchiet, V., Bonnet, G., 2012. A polarization-based FFT iterative scheme for computing the effective properties of elastic composites with arbitrary contrast. Int. J. Num. Meth. Engng 89, 1419–1436.

Monchiet, V., Cazacu, O., Charkaluk, E., Kondo, D., 2008. Macroscopic yield criteria for plastic anisotropic materials containing spheroidal voids. Int. J. Plast. 24, 1158–1189.

Moulinec, H., Silva, F., 2014. Comparison of three accelerated FFT-based schemes for computing the mechanical response of composite materials. Int. J. Num. Meth. Engng 97, 960–985.

Moulinec, H., Suquet, P., 1998. A numerical method for computing the overall response of nonlinear composites with complex microstructure. Comput. Methods Appl. Mech. Engrg. 157, 69–94.

Nervi, J.E.R., Idiart, M.I., 2015. Bounding the plastic strength of polycrystalline voided solids by linear-comparison homogenization techniques. Proc. R. Soc. Lond. A 471, 20150380.

Partridge, P.G., 1967. The crystallography and deformation modes of hexagonal close-packed metals. Metall. Rev. 12, 169–194.

Paux, J., Morin, L., Brenner, R., Kondo, D., 2015. An approximate yield criterion for porous single crystals. Eur. J. Mech. A/Solids 51, 1–10.

Rice, J.R., Tracey, D.M., 1969. On the ductile enlargement of voids in triaxial stress fields. J. Mech. Phys. Solids 17, 201–217.

Rosen, J.B., 1960. The gradient projection method for nonlinear programming. Part I. Linear constraints. SIAM J. Appl. Math. 8, 181–217.

Sarma, G.B., Radhakrishnan, B., Zacharia, T., 1998. Finite element simulations of cold deformation at the mesoscale. Comput. Mat. Sci. 12, 105–123.

Schacht, T., Untermann, N., Steck, E., 2003. The influenceof crystallographic orientation on the deformation behaviour of single crystals containing microvoids. Int. J. Plast. 19, 1605–1626.

Schmidt-Baldassari, M., 2003. Numerical concepts for rate-independent single crystal plasticity. Comput. Methods Appl. Mech. Engrg 192, 1261–1280.

Srivastava, A., Needleman, A., 2013. Void growth versus void collapse in a creeping single crystal. J. Mech. Phys. Solids 61, 1169–1184.

Suquet, P., Moulinec, H., Castelnau, O., Montagnat, M., Lahellec, N., Grennerat, F., Duval, P., Brenner, R., 2012. Multi-scale modeling of the mechanical behavior of polycrystalline ice under transient creep. Procedia IUTAM 3, 64–78.

Tabourot, L., Fivel, M., Rauch, E., 1997. Generalised constitutive laws for f.c.c. single crystals. Mat. Sci. Eng. A234-236, 639–642.

Teodosiu, C., Raphanel, J.L., Tabourot, L., 1993. Finite element simulation of the large elastoplastic deformation of multicrystals, in: Teodosiu, C., Raphanel, J.L., Sidoroff, F. (Eds.), Large plastic deformations, Rotterdam. pp. 153–168.

Tomé, C.N., Kocks, U.F., 1985. The yield surface of HCP crystals. Acta Metall. 33, 603–621.

Tvergaard, V., 1982. On localization in ductile materials containing spherical voids. Int. J. Fract. 18, 237–252.

Vincent, P.G., Suquet, P., Monerie, Y., Moulinec, H., 2014. Effective flow surface of porous materials with two populations of voids under internal pressure: II. Full-field simulations. Int. J. Plast. 56, 74–98.

Willot, F., Pellegrini, Y.P., 2008. Fast fourier transform computations and build-up of plastic deformation in 2D, elastic-perfectly plastic, pixelwise disordered porous media, in: Jeulin, D., Forest, S. (Eds.), Continuum Models and Discrete Systems CMDS 11, pp. 443–449.

Yerra, S., Tekoglu, C., Scheyvaerts, F., Delannay, L., Houtte, P.V., Pardoen, T., 2010. Void growth and coalescence in single crystals. Int. J. Solids Struct. 47, 1016–1029.

Yoo, M.H., 1981. Slip, twinning, and fracture in hexagonal close-packed metals. Metallurgical Transactions A 12A, 409–418.

Zhang, K.S., Bai, J.B., François, D., 2001. Numerical analysis of the influence of the Lode parameter on void growth. Int. J. Solids Struct. 38, 5847–5856.